Universiteit Utrecht

Theoretical Physics & Mathematical Sciences

Phase transitions in the granular hard hexagon model

Master Thesis

Lorenzo Sierra Perez

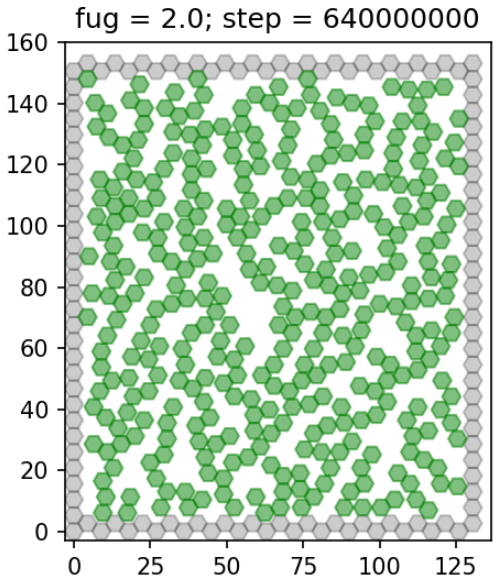

Supervisors:

Dr. Cristian Spitoni
Mathematical Institute

Prof. Dr. René van Roij
Institute for Theoretical Physics

10-08-2021

Abstract

We studied granular matter by looking at a two-dimensional hard hexagon model with added granular constraints. In the equilibrium model, we proved the existence of a phase transition by using Peierls' argument, with an ordered phase at high densities, and provided a numerical argument for a disordered phase at low densities. We also studied the non-equilibrium granular hexagon model numerically, and found the system highly sensitive to the parameters describing gravity and friction.

Contents

1 Introduction

Granular matter is without a doubt an important, omnipresent factor in our lives. It inhabits a powerful place in most of our industries, such as pharmaceutics, construction and agriculture. They help shape our planet by playing an essential role in processes like landslides, erosion and sedimentation. Practically everything we eat or drink has been part of a granular matter somewhere in the process of creating the foodstuff. It is then easy to see why we'd be so interested understanding the behaviours of granular matter.

On the surface there is a lot of overlap between equilibrium thermodynamics and the physics of granular matter. If we take e.g. sand in water, which is a granular matter, a sand pile can exist between a volume fraction of around 0.57 and 0.74, with the random close packing density at around 0.64. Below this volume fraction, the sand is quite disordered. Above the volume fraction however, we start to see more and more crystalline structure in the sand pile, with larger clusters for a higher density. This roughly mirrors the behaviour of equilibrium fluids around their freezing points. In contrast to molecular systems, however, the positions of individual particles in a granular system can be tracked in experiment [Rie+18].

A logical step would then be to use a theoretical model that somewhat mirrors a model from equilibrium statistical mechanics, and indeed it has been shown by Edwards[EO89] that the large scale behaviours of granular matter fit into the statistical mechanics structure. His model of granular matter consists of a simple change in the hard sphere model; the model only allow configurations that are mechanically stable, i.e. arrangements where the particles can remain at rest under the influence of confining forces (e.g. gravity, friction), with no overlap between the particles. This approach seems reasonably justified for static granular matter[Sch+07], and is conjectured to behave like the hard sphere model [Rad07], which is supported by [AR10].

The general model we will discuss is a variation of the equilibrium model for hard hexagon lattice gas[Bax16; HP73]. This is a two-dimensional lattice model of a gas of hard molecules within the framework of the grand canonical ensemble, where two particles cannot be directly adjacent to each other or lying on top of each other. We see each particle as the centre of a hexagon, meaning that we place hexagons with a radius of the same size as the lattice spacing in such a way that the hexagons do not overlap. The hard hexagon model is a well known model, and was first solved by Baxter[Bax16] in 1980, via the use of transfer matrices and the Rogers-Ramanujan identities. Before that, however, Heilmann et al. [HP73] had already shown that there exists a phase transition in the model by appropriating the Peierls' argument -originally used for the Ising model- and applying it to the hard hexagon model.
As the hard hexagon model is a grand canonical model, the total number of hexagons in the system can vary, and is fixed by a chemical potential. In the hard hexagon model, all valid states have zero energy, which means that the only important control variable is the ratio of the chemical potential to the temperature, or $\mu\beta$. The exponential of this ratio

$$z = e^{\mu\beta}, \tag{1}$$

is called the 'activity'. Obviously, the larger the activity, the denser configurations are. If we

have a triangular lattice of N sites, we get a grand grand partition function that looks like

$$Z = \sum_{n=0}^{N/3} z^n g(n, N), \tag{2}$$

with $g(n, N)$ the number of ways of placing n particles on the lattice, such that no two are adjacent. We then define the function κ by

$$\kappa(z) = \lim_{N\to\infty} Z(z)^{1/N}, \tag{3}$$

as a function of the activity. κ functions as the partition function per lattice site, so that $\log(\kappa)$ will be the free energy per lattice site.
We can relate the model -it being a hexagon lattice gas- to the Ising model by rewriting the partition function as follows. We introduce a 'spin' σ_i for each lattice site i, where $\sigma_i = 0$ if there is no particle at site i, and $\sigma_i = 1$ if there is a particle. We can then write (2) as

$$Z = \sum_{\sigma} z^{\sigma_1+\ldots+\sigma_N} \prod_{(i,j)} (1 - \sigma_i\sigma_j), \tag{4}$$

which is very similar to the nearest-neighbour Ising model. This provides us with some argument for the reasoning why Dobrushin, after proving phase transitions in 2-d and 3-d Ising models using the Peierls' argument [Dob65], went on using it to prove the same in lattice gas models [Dob67], and why Heilmann applied it to the hard hexagon lattice model. The parallel between a ferromagnetic zero-magnetic Ising model, with symmetry between the up and down states, and the simple cubic lattice, with symmetry between the two sublattices of the lattice, should be noted, as it makes the proof immediately applicable to the cubic lattice. For the triangular and heagonal lattices, however, this quick application of the argument does not work, as there are now more distinct sublattices that can be mapped into any of the other sublattices by translation.

To talk about granular behaviour using the hard hexagon model, we follow Edwards by adding gravity and friction to the model. We can still use the Peierls' argument to prove a phase transition for high densities, but now low densities give us a problem, as granular matter does not exist at low densities. We follow Radin [Rad07] in modelling this system to provide a numerical argument for the assertion that granular matter and our model are disordered at a low density. We do this by running a Markov chain Monte Carlo simulation on the model for different densities. This will all be discussed in Sec. 1.

After discussing the above equilibrium model for granular matter, we focus on a non-equilibrium variation of our model, discussed in Sec. 2. We let each hexagonal particle follow a random walk, where we biased moving down positively (as to mimic gravity) and turned the random walk lazy whenever a particle is touching another particle, making it harder to separate again (as to mimic friction).

Part 1
Equilibrium Model

In this section, we discuss the models we will be working with throughout the equilibrium part of the thesis, and the method we will use to prove phase transitions.
The general form of our model is an equilibrium model of congruent hard hexagons on a triangular lattice, with the edges of the hexagons a multiple of the lattice spacing [AR10; Bax16; HP73; LY52]. We will talk about the addition of gravity and friction effects to the model later; first we will take a closer look into the model and proving phase transitions in the model without gravity and friction constrictions, outlined by Heilmann [HP73].

1 The Non-granular Hard Hexagon Model

The base model from which we will build onwards is the two-dimensional lattice model of a gas of hard congruent hexagonal particles, where the lattice is the triangular lattice. This model is both discussed by Heilmann and Praestgaard [HP73] and by Baxter [Bax16].
We start with an infinite triangular lattice Λ. The contours of the hexagons are confined to the lattice points. The hexagons are oriented such that the edges of the hexagons are parallel to the edges of the lattice. The length of the sides (and radius) of the hexagons is a fixed integer multiple of the lattice spacing. We will call this integer s. For the rest of the thesis we will use $s > 1$, so the hexagon side length is bigger than the lattice spacing. We can also consider the 'area' of the lattice; if we connect all the lattice points with their neighbours, we split the area into small triangles, which we will call elementary triangles.

We count the number of lattice points that are contained inside a hexagon by counting the amount of distinct hexagonal tilings on the lattice, which gives us a total of $M = 3s^2$ lattice points. This way of counting means that every lattice point inside the hexagon corresponds uniquely to a sublattice. These M lattice points correspond to the M distinct sublattices, which we define as collections of hexagons which tile the plane. There is a fixed boundary in place, consisting of hexagons which intersect their neighbours in full faces, making them all lie on the same sublattice, which we call the boundary sublattice. The space enclosed by this boundary is called $V \subseteq \Lambda$. We call the area not covered by hexagons in V as $V_{\text{no hex}}$.
We are situated in the grand-canonical ensemble, meaning that we have the grand canonical probability measure on the subsets of the set of all possible configurations, and where the probability of seeing a configuration with n particles in the fixed volume V is proportional to $\left(e^{\beta\mu}\right)^n$, with $\mu \in \mathbb{R}$. Here $e^{\beta\mu}$ we will call the activity of a hexagon. The probability measure on V we will call m_V, where

$$m_v(\mu) = \frac{e^{\mu\beta n}}{Z_V}, \tag{5}$$

where Z_n is the appropriate normalisation. We let m be the weak limit of m_V as $|V| \to \infty$. This measure will be unique for small μ and thus small activity, and for large positive μ, the measure depends on the boundary conditions. This hints at a phase transition between a low and high density phase, where we find an ordered state sensitive to the boundary for a large μ and a disordered state for low μ. This last statement we will prove in the following sections.
Now that we defined the model, we will now discuss the concepts needed for using the Peierls' argument. The different states will be defined by the different ways to tile the lattice with the

hexagons, which is decided by the number of sublattices of the lattice. This means that we have M different, distinct states, or tilings, that are possible in our system. This means that we have $\frac{M(M-1)}{2}$ different types of Peierls' contours. Furthermore, if in a configuration there is a void large enough to fit additional hexagons, we will fill the void up by placing 'virtual hexagons'. With this in place, we can assume that no configuration contains a void large enough to accommodate a hexagon. The problem of distinguishing between virtual and real hexagons will be considered later.

Let us define the following terms

Definition 1.1. *We define the edge set E as*

$E := \{\lambda \in \Lambda : \lambda$ *is a shared part of two hexagons belonging to different tilings (structures)*$\}$.

Using this and $V_{\text{no hex}}$, we define the following:

Definition 1.2. *An element of contour is any element of the set*

$$\overline{V_{no\ hex}} \cup E,$$

meaning that an element of contour is either a lattice point not covered by a hexagon or the lattice point is shared by two hexagons of different tiling/structure.
A contour C is a connected component of the set of all elements of contour.

We note that the above definitions allow for contours inside of other contours.

Definition 1.3. *The area $A(C)$ of a contour C equals one-half the number of elementary triangles constituting the empty area of the contour.*

As stated before, the boundary of our system is fixed. We will call the corresponding boundary structure A. Again, a point inside the boundary that is not covered by a hexagon of the A structure must then be surrounded by a contour, or must be part of a contour. We can look only at outer contours (i.e. contours that are not themselves surrounded by other contours), as they will be surrounded by the A structure.
A contour in this model can be specified as the following. Imagine a plane of hexagons of the boundary structure A. The edges of the hexagons create a hexagonal lattice. We can now create a hole in this structure, where the hole is a self-avoiding polygon on this hexagonal lattice. This polygon, which we will call B, constitutes then the boundary between the outer A structure and the contour. We then describe the positions of all the hexagons next to the boundaries of the hole. With this, we have specified the outer boundary between A and the contour, and the inner boundaries between the contour and the different structures that are found inside.
A contour C splits the interior hexagons into different regions which are separated from the exterior structure A and from each other. These regions are called C-interior regions. We note that the structure of the hexagons that are positioned adjacent to C will all have the same structure, which we will call the boundary structure of the region.

It should be noted that this system differs heavily from the Ising model where the Peierls' argument originally was used. Let us convince ourselves first and foremost that we can use the Peierls' argument for this system. Two possible problems that come to mind is that we need to make rigorous the deletion of terms in the partition function when upper bounding the probability of a contour, and secondly we need to address the fact that now we work with M different substructures, instead of two as in the Ising model. Let us start with the first problem.
As we know, in the Peierls' argument we get the probability of finding a contour C in a system that is

$$p(C) = \frac{\sum_{\omega:\omega\ni C} w(\omega)}{\sum_{\omega} w(\omega)}, \tag{6}$$

where $w(\omega)$ is the canonical weight of a configuration ω, and the denominator is the total partition function. We would like to delete terms in the partition function such that we get a one-to-one relationship between terms in the numerator and in the denominator.
Let us first assume two possible local structures A and B - the problem of more structures will be handled in our second point. We already defined how to draw contours between the different structures, and we note that a configuration can be specified uniquely by specifying all the contours. The contribution of a contour is proportional to the 'length' of the contour. Furthermore there exists a reflection which maps the lattice onto itself while interchanging the two local structures. We now consider contour C which has A-structure on the outside and B-structure on the inside, and our goal is to make a one-to-one correspondence between configurations with C and configurations where C is not present. For that, we define a C-1 contour as any contour that is inside C, but not inside any other contour that is also inside C. The set of all C-1 contours we call $\mathcal{F}(C)$.

To transform a configuration with contour C into a configuration without C, we can remove some elements of $\mathcal{F}(C)$, and divide the rest into regions which are invariant under a reflection. We start by associating with every element of $\mathcal{F}(C)$ a line of reflection. For a contour in $\mathcal{F}(C)$, this line crosses that contour, and its position relative to the contour is invariant under translation and reflection of the entire lattice. The set of elements of $\mathcal{F}(C)$ which are reflected like this we will call K, and we will call T the set of elements to be deleted, i.e. $T = \{C\} \cup \mathcal{F}(C) \backslash K$. If we divided the elements correctly into these two sets, then we get a set $\mathcal{M}$ of non-overlapping regions, where each region has an associated reflection line that maps the region onto itself, and each member of K should be completely inside a member of $\mathcal{M}$. This division is done via starting with imperfect sets $T_0 = C$ and $K_0 = \mathcal{F}(C)$, and improving T_i, K_i every step. $\mathcal{M}_i$ is then a set of regions such that every region has an associated reflection line, mapping that region onto itself, and each region is connected and each member of K_i is associated with a member of $\mathcal{M}_i$ which is totally inside. The exact process of purifying these sets can be found in [Hei74]. This process is also reversible, as shown in the corresponding paper.

Now coming back to our probability equation (6), we can talk about which terms to delete and which to keep in the denominator. We can then split the summation over the configurations containing C in three parts: the summations over the possible configurations outside C,

which we will call ext(C); the summation over T-contours containing C as the outer contour, so $T \ni C$; and the summation over configurations inside C, which are consistent with T, which we call int(T). For a fixed T, we then keep the following terms in the denominator: the sum over ext(C) is kept unchanged, while in the sum over int(T) for each term that we find in the numerator, we get the corresponding term in the denominator by reflecting the configuration inside each region in $\mathcal{M}$ and then deleting T. If this transformation does not cause a term in the denominator to correspond to two or more terms in the numerator, we are able to write

$$p(C) = \frac{\sum_{\omega:\omega\ni C} w(\omega)}{\sum_{\omega} w(\omega)} \leq \sum_{T:T\ni C} \frac{\sum_{\text{int}(T)} e^{\beta\epsilon L(C)}}{\sum_{\text{int}(T)} e^{\beta\epsilon(L(C)+L(T))}} = \sum_{T:T\ni C} \exp\{-\beta\epsilon L(T)\}, \tag{7}$$

where ϵ is a lower bound on the 'energy' per unit length of a contour, and $L(T)$ is the total length of contours in T. This is the necessary step we want to achieve in the Peierls' argument. As the process of getting T, K, and $\mathcal{M}$ is reversible, we see that the correspondence between the terms in the numerator and in the denominator is indeed one to one. This means that our deleting of the terms in the partition function is accounted for.
Coming to the second problem, the triangular lattice gives us at least three local structures. This is solved by treating each of the interior regions separately, as in that case we can talk about two structures again, namely an 'inside' and 'outside' structure. We do get left with one problem when we try to delete a C-1 contour, as the structure of a C-1 contour does not need to be the same as the structure outside of C. This can be easily solved by treating the interior of the C-1 contour which gets deleted as the interior of C. With both of these discussions we have taken care of the problems, and are free to use the Peierls' argument with this in mind.

Continuing with our setup, we want to start saying something about the probability of belonging to the A structure. Let us define the following:

Definition 1.4. *The probability $p_A(x)$ for a given point $x \in L$ gives the probability that the point x is not covered by a hexagon belonging to the A structure.*

With this, and our above discussion of the model, we can finally pose the theorem we are going to prove:

Theorem 1.1. *For the non-granular hard hexagon model, and for sufficiently large activity z, and x a point on the lattice, we have that $1 - p_A(x) > (3s^2)^{-1}$, that is, a hexagon covering x will not be centred equiprobably on each of the $3s^2$ sublattices.*

This means that for a large enough activity z, the boundary starts influencing the positions of the hexagons in the system. This implies the following corollary:

Corollary 1.1. *There exists an order-disorder phase transition in the non-granular hard hexagon model.*

For small z, the model is in a disordered state, and for large enough z it is in an ordered state.
Now we can go into proving this theorem.

1.1 Proof Theorem 1.1

We first notice that there are three possibilities of a lattice point x not being covered by a hexagon belonging to the A structure: either there is no hexagon covering x, the hexagon covering x belongs to a different structure, or x is covered by a virtual hexagon that is of the A structure. This means that x is either part of a contour or there is an outer contour around x. We can thus upper-bound our probability $p_A(x)$ by the probability that point x is surrounded by or part of a contour C, plus the probability that x belongs to a virtual hexagon that is of the A structure. We define the following:

Definition 1.5. *The probability $\tilde{p}(x)$ for a given point $x \in L$ gives the probability that point x is either surrounded by a contour or part of a contour.*

Definition 1.6. *The probability $p_v(x)$ for a given point $x \in L$ gives the probability that point x is covered by a virtual hexagon that belongs to the boundary structure A.*

We can now write

$$p_A(x) \leq \tilde{p}(x) + p_v(x). \tag{8}$$

Let us first focus on the probability that a point x is surrounded or covered by a contour. As we are in the grand canonical ensemble, the grand canonical partition function is

$$Z = \sum_i e^{n_i \mu \beta}, \tag{9}$$

where i sums over all possible individual configurations i, each with particle number n_i. The probability of a certain configuration j is then given by

$$p(\text{configuration } j) = \frac{e^{n_j \mu \beta}}{Z}. \tag{10}$$

If we now want to know the probability of a given outer contour C, this will be given by

$$p(C) = \sum_{i : i \ni C} \frac{e^{n_i \mu \beta}}{Z}, \tag{11}$$

summing over all the configurations that contain C as outer contour. As we are using the Peierls' argument, we want to upper bound this probability by 'deleting' terms in the grand-partition function to get a one-to-one correspondence with terms in the numerator and in the denominator. We get this one-to-one correspondence as follows. Let us consider a configuration with outer contour C, where the contour has area $A(C)$. Per C-interior region, we translate the hexagons of that C-interior region such that the boundary structure of the region turns into the A structure. We can do this for all C-interior regions, and furthermore we can translate them all in a similar direction, i.e. one of two directions that are 60°rotated from each other, such that no translated hexagons are overlapping. Because conservation of area, the same total area of $A(C)$ is uncovered, but now all the heaxgons around this uncovered area are of structure A, so we can fill the hole with new hexagons of structure A. The system then gains $A(C)/M$ hexagons.

These new configurations with $A(C)/M$ more hexagons are the terms in the denominator that we do not delete, and we throw away the rest. This results in an upper bound for $p(C)$:

$$p(C) \leq \frac{\sum_{i:i\ni C} e^{n_i \mu\beta}}{\sum_{i:i\ni C} e^{(n_i + A(C)/M)\mu\beta}} = e^{-A(C)\mu\beta/M}. \tag{12}$$

With this, we can get an expression for $\tilde{p}(x)$:

$$\tilde{p}(x) = \sum_{C:C\ni x} p(C), \tag{13}$$

where the sum runs over all C such that x is inside the outer boundary B of C. With our previous discussion in mind, we can upper bound this by

$$\tilde{p}(x) = \sum_{C:C\ni x} e^{-A(C)\mu\beta/M}. \tag{14}$$

We now want to introduce a distinction between outer boundaries and inner hexagons next to C, so we write the above as

$$\tilde{p}(x) = \sum_{B:B\ni x} S(B), \tag{15}$$

where we sum over all outer boundaries B with the property that point x is inside of B, and where

$$S(B) = \sum_{\text{inner hex}} e^{-A(C)\mu\beta/M}, \tag{16}$$

where we sum over all the inner hexagons next to C.
To make life easier, we want to split up this $S(B)$ again as a summation over the outer inner hexagons (the hexagons nearest to the boundary B) and the rest:

$$S(B) = \sum_{\substack{\text{outer}\\ \text{inner}\\ \text{hexagons}}} \sum_{\substack{\text{inner}\\ \text{inner}\\ \text{hexagons}}} e^{-A(C)\mu\beta/M}. \tag{17}$$

The shape of B decides the amount of outer hexagons in the configuration. The maximal amount of outer hexagons for B we will call n. The first sum in (17) will then be over the possible position coordinates of hexagons $1, \ldots, n$. We write the position coordinates as $j(1), \ldots, j(n)$. In similar fashion, the amount of inner inner hexagons is determined by the shape of B, and we denote the maximal amount of these hexagons as m. The second sum in (17) will then be over $j(n+1), \ldots, j(n+m)$. We can then write $S(B)$ as

$$S(B) = \sum_{j(1)} \cdots \sum_{j(n+m)} e^{-A(C)\mu\beta/M}. \tag{18}$$

The value of $A(C)$ depends on both B and all the position coordinates $j(1), \ldots, j(n+m)$. We want to divide the total $A(C)$ into contributions from each of the $n+m$ hexagons inside B. We do this by taking the hexagon-sized areas next to B such that it corresponds to a tiling of A-structured hexagons. We then see in that in every such an area, there can be either

one or none hexagons placed. For a given position of the placed hexagon, the uncoverable area is calculated as if no other hexagon in the system has been placed, only counting inside the hexagon-sized area. Then we also include uncoverable area outside of this hexagon-sized area if it is certain that it cannot be made uncoverable by placing another hexagon. Using this convention, which will be worked out in much more detail later on, we can write

$$A(C) = \sum_{i=1}^{n+m} a_i, \tag{19}$$

where a_i is the contribution of hexagon i to $A(C)$. Under the area-contribution rules, a_k is independent of the position $j(l)$ for each hexagon $l > k$. Then, introducing

$$b_{j(i)} = e^{-a_i \mu M \beta}, \tag{20}$$

we can rewrite $S(B)$ and (18) as follows:

$$S(B) = \sum_{j(1)} b_{j(1)} \cdots \sum_{j(n+m)} b_{j(n+m)}. \tag{21}$$

We now note that in the case that we cannot place all $n + m$ hexagons in a configuration (as both n and m are the maximal amount of hexagons), for every hexagon i that we cannot place, we take $a_i = 0$ and $\sum_{j(i)} b_{j(i)} = 1$.
We will now show an upper bound for $\sum_{j(i)} b_{j(i)}$ for $i > n$.

Lemma 1.1. *We can bound* $\sum_{j(i)} b_{j(i)} \leq \max\{\delta(\mu M \beta, s), 1\}$ *for* $i > n$*, where delta and for fixed values of the positions of the preceding hexagons* $j(1), \ldots, j(i-1)$.

Proof Lemma: Within the sum over the positions of the inner inner hexagons, we place the hexagons in a fixed order such that hexagons are placed close to already fixed hexagons to enlarge the uncoverable area as much as possible. This means that we stepwise continue the creation of the contour C in question. According to the area-contribution rules, the area we attribute to an inner inner hexagon is obtained by placing this hexagon relative to two preceding ones, as seen in Fig. 2. Based on the symmetry of the lattice, we can talk about six principal positions of these two preceding hexagons. These six positions correspond to the leftmost corner of the second hexagon being placed in one of the six triangles seen in Fig. 1. Following the area-contribution rules, the case that the second hexagon has its leftmost point in triangle VI gives us the largest value of $\sum_{j(i)} b_{j(i)}$.
For placing the third hexagon, we again get a lot of principally different positions, as we can see in Fig. 3. The u and v signify the relative position of the two preceding hexagons compared to the closest starting position of triangle VI.
The third hexagon will bring two additional coordinates x, y that signify the relative position of the third hexagon compared to the same point as above. We can then calculate the uncoverable area that we contribute to the placing of the third hexagon using these coordinates. For the first 8 positions, we can split the uncoverable area into four subareas, which can be

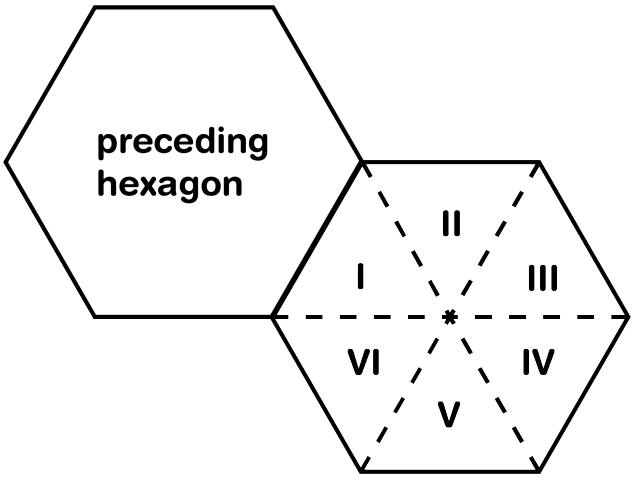

Figure 1: The six principally different positions a placed hexagon can have depending on in which region the upper left corner of the hexagon is placed.

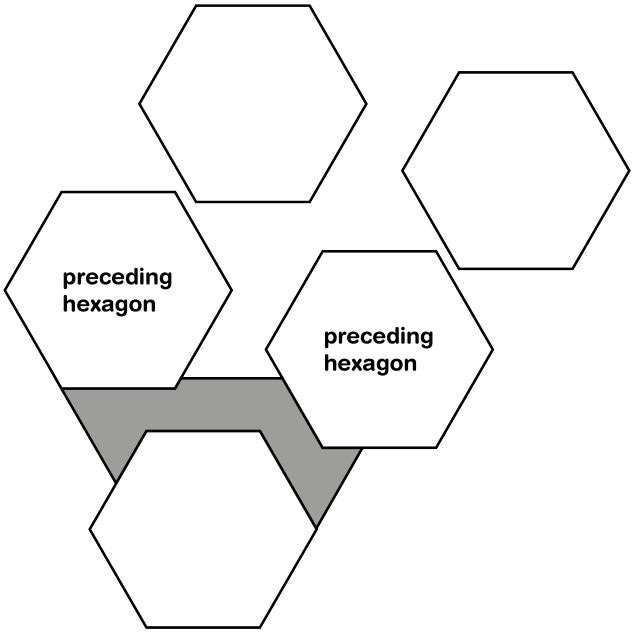

Figure 2: The uncoverable area (shaded) obtained by placing a hexagon next to two preceding hexagons.

seen in Fig. 4, and give us the following area

$$a = \frac{1}{2}(v-x)^2 + y(v+s) + x(s+u-v) + \frac{1}{2}(u-y)^2 \tag{22}$$

$$= \frac{1}{2}u^2 + \frac{1}{2}v^2 + x(s+u-v) + y(s-u+v) + \frac{1}{2}(x-y)^2. \tag{23}$$

For the rest of the positions (e.g. position 9, as seen in Fig. 5), we can see that at least one

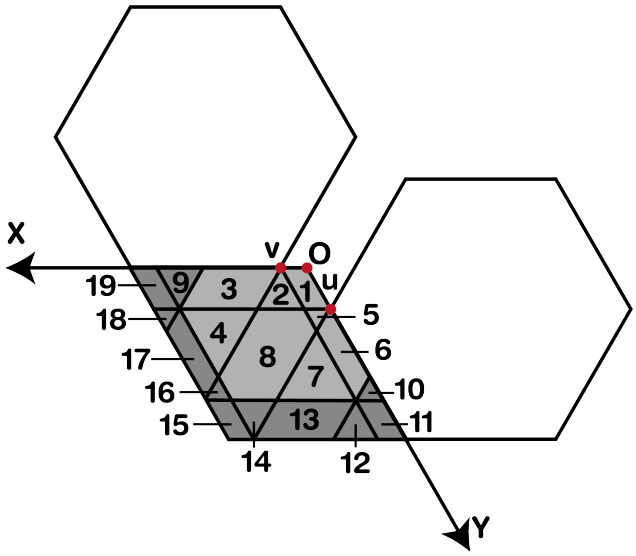

Figure 3: The two preceding hexagons are placed in situation VI. We define the relative position with coordinates u and v. The numbered regions correspond to different positions of the next hexagon, provided that the position is defined by the position of the upper right corner. The lighter shaded region leads to the same upper bound on the area, and the darker shaded region leads to another upper bound.

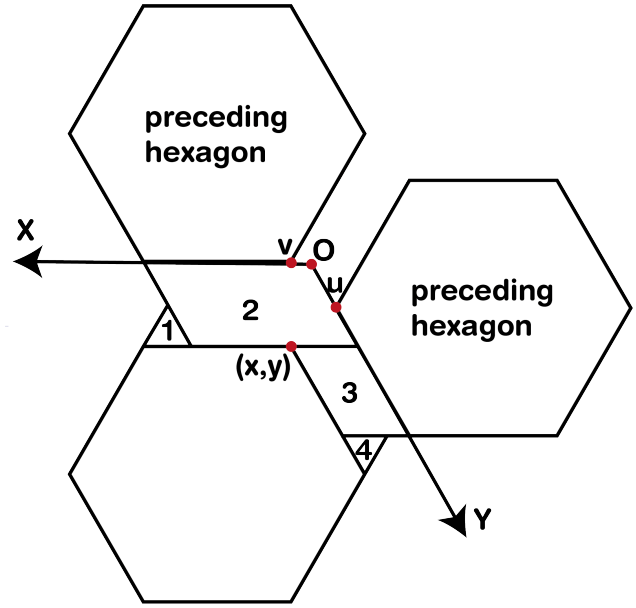

Figure 4: The two preceding hexagons are placed as in case VI, and the next hexagon is placed in position 4 as seen in Fig. 3. The position of the third hexagon, marked by position of the upper right corner of the hexagon is given by coordinates x, y. The uncoverable area is divided in four numbered regions.

triangle with side s can be placed in the uncoverable area, meaning that for these positions

$$a \geq \frac{1}{2}s^2. \tag{24}$$

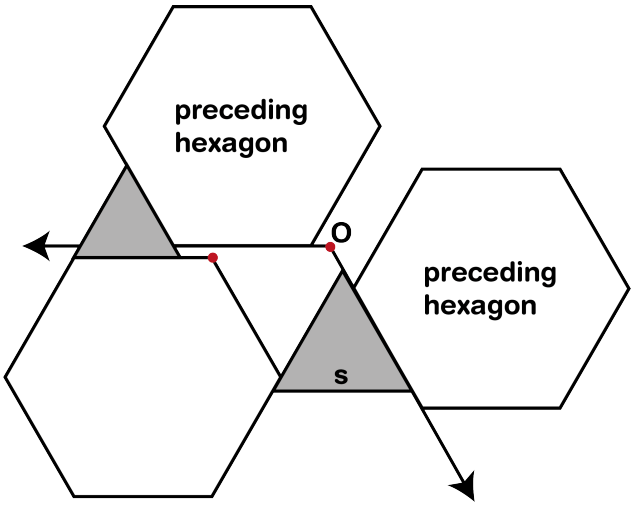

Figure 5: The preceding hexagons as in case VI and the third hexagon placed in position 9 as in Fig. 3. The uncoverable area (shaded) exceeds $\frac{1}{2}s^2$.

The total number of positions leading to position 2 is less than $5s^2$. One should note that for $u = v = 0$, meaning that we can always place a hexagon
As we discussed the possible positions and their respective uncoverable area contribution, we can sum them all together and extend the upper limit to infinity to upper bound $\sum b$:

$$\sum_{j(i)} b_{j(i)} \leq \sum_{x=1}^{s}\sum_{y=1}^{s}\left(e^{-\frac{\alpha}{2}(u^2+v^2)}e^{-\alpha(x(s+u-v)+y(s-u+v)}\right) + 5s^2e^{\frac{\alpha}{2}s^2} \tag{25}$$

$$= \left(e^{-\frac{\alpha}{2}(u^2+v^2)}(1-e^{-\alpha(s+u-v)})^{-1}(1-e^{-\alpha(s-u+v)})^{-1}\right) + 5s^2e^{-\frac{\alpha}{2}s^2} \tag{26}$$

$$\tag{27}$$

where $\alpha = \frac{\mu}{MkT} = \frac{\mu}{3s^2kT}$. Now, we can upper bound this further by realising that for the first term, either $u > 1$ or $v > 1$, as for $u = v = 0$ we'd be in the second term:

$$\sum_{j(i)} b_{j(i)} \leq \left(e^{-\frac{\alpha}{2}}(1-e^{-\alpha(s+1)})^{-1}(1-e^{-\alpha(s-1)})^{-1}\right) + 5s^2e^{-\frac{\alpha}{2}s^2} \equiv \delta, \tag{28}$$

This final expression is what we call δ.
As stated before, when a hexagon can't be placed, a_k becomes 0 which corresponds to $\sum_{j(k)} b_{j(k)} = 1$, hence we can upper-bound $\sum_{j(i)} b_{j(i)} \leq \max\{\delta(\beta\mu/M, s), 1\}$, proving the lemma. ■

Using (21) and Lemma 1.1, we can find that

$$S(B) \leq 1 \cdot \sum_{j(1)} b_{j(1)} \cdots \sum_{j(n)} b_{j(n)}, \tag{29}$$

provided that $\delta \leq 1$. This means that we upper-bounded $S(B)$ with the positions of only the outer inner hexagons. To find our probability in (15), we need to both get an expression for

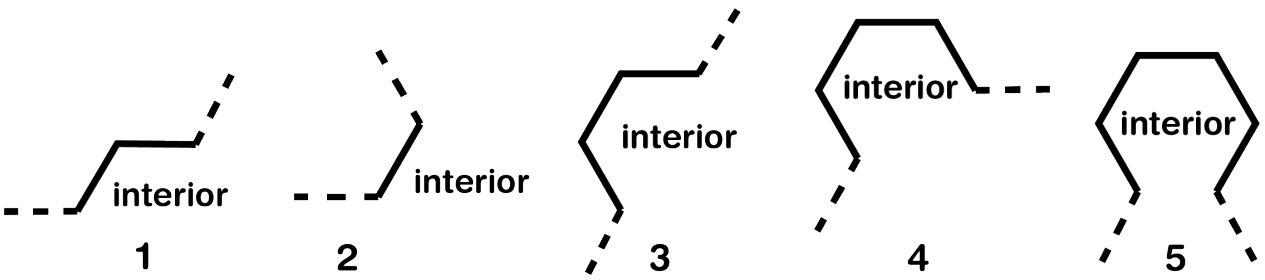

Figure 6: The five types of segments that make up outer boundary B. The segment is emphasised by a thick line, where the dashed lines show the continuation of the boundary.

the sum over all B containing point x, and an expression for $S(B)$, where we know that we now only have to care about outer inner hexagons. The placing of these hexagons depends directly on the shape of the outer boundary B. We established previously that B is a self-avoiding polygon on a hexagonal lattice, and this means that we can consider it to be made up out of five different types of boundary segments, which can be seen in Fig. 6.
As we fill any void big enough with a virtual hexagon, we see in that boundary type 5 cannot happen in our system, as a virtual hexagon would fill the void. The length of boundary B we will call l, which measures the length of B in units of hexagons. Let $\eta(i)$ be the number of segments of type i we can find in a boundary, then we see that

$$l = 2\eta(1) + \eta(2) + 3\eta(3) + 4\eta(4). \tag{30}$$

Now let's talk about upper-bounding the total amount of boundaries containing a fixed hexagon.

Lemma 1.2. *The number of boundaries B with a given length l surrounding a fixed hexagon ν is less than $\nu(l)$, where*

$$\nu(l) = \left(\frac{3 \cdot 2^{l-2}}{l}\right)\left(\frac{1}{48}l^2 + \frac{1}{4}\right). \tag{31}$$

Proof Lemma: We can split our expression for $\nu(l)$ up into the two bracketed terms, where (i) the first is an upper bound on the number of shapes of B for a given l, and (ii) the second is an upper bound on the number of hexagons that can be inside a polygon of length l. As we work on a hexagonal lattice, we know that l has to be even. Let us start with proving (i):

As we are on a hexagonal lattice, there are three directions to go to from a starting point. After that, for $l-2$ parts we have two directions to go to, as we cannot go back. For the last part, we only have a single direction we can choose, as B should be a closed boundary. The final part then has to go in the direction such that we end up at the starting point again. This gives us the term in the numerator $3 \cdot 2^{l-2} \cdot 1$. As there are l possible starting points for the same boundary B of length l, we divide this term by l, giving us the first term in (31).

To prove (ii), we first see in that for $l = 6$, we get that

$$\frac{36}{48} + \frac{1}{4} = 1, \tag{32}$$

as we expect. Furthermore, the point at which the smallest possible increase of l, so $l \mapsto l+2$, is bigger than 48, is for $l = 12$, $l + 2 = 14$. This means that after this, the smallest increase of l will result in the upper bound going up at least 1, making sure that it upper-bounds a possible extra hexagon inside the boundary. We then only need to check if our term is a sufficient upper bound for $6 < l < 14$. We easily see that the only two possibilities of having a polygon with $6 < l < 14$ are for $l = 10$, holding 2 hexagons, and $l = 12$, holding 3 hexagons. It's easy to see that

$$\frac{1}{48}10^2 + \frac{1}{4} > 2, \tag{33}$$

and

$$\frac{1}{48}12^2 + \frac{1}{4} > 3, \tag{34}$$

showing that the bound is sufficient for $6 < l < 14$. Putting all of this together, we see that the second term in the lemma statement is indeed an upper-bound for the amount of possible hexagons inside of boundary B with length l. This proves (ii).
As both (i) and (ii) are proven, we have proven the lemma. ■

In general, we can place one outer inner hexagon outside of each segment. There is one caveat, as a hexagon outside of segment type 2 will technically be regarded as an inner inner hexagon. For the other types, we get the following bounds

$$\sum_{j(i)} b_{j(i)} \leq \gamma_k(\beta\mu/M, s), \quad i \leq n, \tag{35}$$

where k refers to the type of the segment to which the ith hexagon is located.

Lemma 1.3. *The γ_k bounds are as follows:*

$$(i) \quad \gamma_1 = \frac{e^{-\alpha s}(2 - e^{-\alpha s})}{(1 - e^{-\alpha s})^2} + 2s^2 e^{-\alpha s^2} \tag{36}$$

$$(ii) \quad \gamma_3 = \frac{e^{-2\alpha s}(2 - e^{-2\alpha s})}{(1 - e^{-2\alpha s})^2} + 2s^2 e^{-2\alpha s^2} + e^{-\frac{3}{2}\alpha s^2} \tag{37}$$

$$(iii) \quad \gamma_4 = \frac{e^{-2\alpha s}}{1 - e^{-2\alpha s}}, \tag{38}$$

Proof Lemma: (i) Let us start by considering γ_1, so placing a hexagon near boundary type 1, as seen in Fig. 6. We can visualise the possible placements as in Fig. 7, where each of the six numbered regions result into a different shape of the uncoverable area, provided that the position of the placed hexagon is given by the position of the upper left corner. The two cases I and II will give the same contribution because of symmetry.
Let us consider a hexagon in situation I, this is seen in Fig. 8. We see that the uncoverable area we find is (in the order seen in the figure)

$$a = xy + \frac{1}{2}y(2s - y) + x(s - y) + \frac{1}{2}y^2 \tag{39}$$

$$= s(x + y). \tag{40}$$

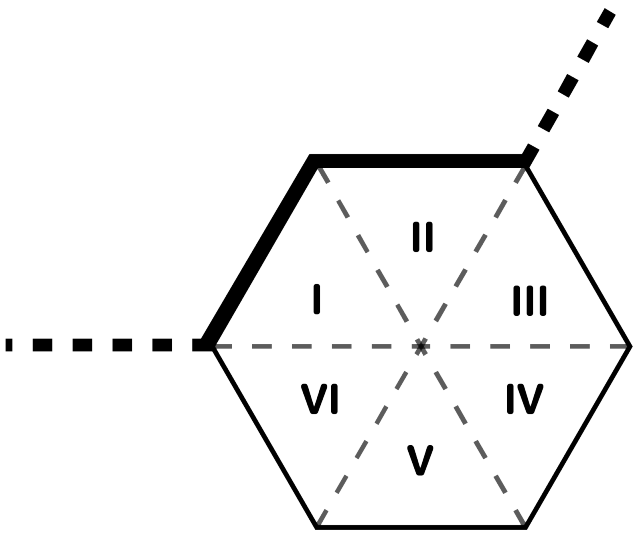

Figure 7: A segment of type 1, denoted by thick lines. The thick dashed lines show the continuation of the boundary. The six regions I-VI correspond to the six principally different positions the hexagon can be in, depending on where the upper left corner of the adjacent hexagon is placed.

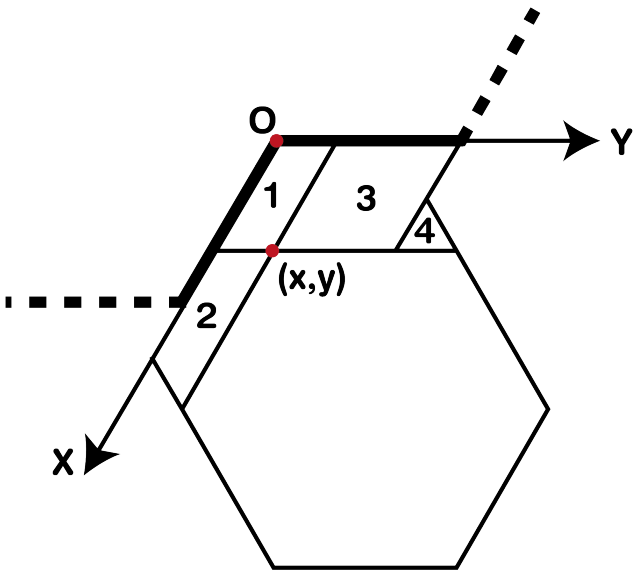

Figure 8: A segment of type 1 and the placed hexagon in a case I position. The uncoverable area is divided in four different regions.

For cases III-VI, we can see in Fig 7 that we will get an uncoverable area of at least s^2, as triangles I and II will be uncovered. Lastly, there could also not be any hexagon placed, resulting again in an uncoverable area of at least s^2 that is not attributed to another hexagon. We can then upper bound $\sum b$ by

$$\sum_{j(i)} b_{j(i)} \leq \sum_{x=1}^{s} \sum_{y=1}^{s} \left(e^{-\alpha s(x+y)}\right) + 2s^2 e^{-\alpha s^2} - 1, \tag{41}$$

where we pick up the minus one from the fact that the position $x = y = 0$ is not allowed, as this would mean that the hexagon is of the A-structure. We can remove the sum by letting it go to infinity and then

$$\sum_{j(i)} b_{j(i)} \leq \frac{1}{(1-e^{-\alpha s})} \cdot \frac{1}{(1-e^{-\alpha s})} - 1 + 2s^2 e^{-\alpha s^2} \tag{42}$$

$$= \frac{e^{-\alpha s}(2-e^{-\alpha s})}{(1-e^{-\alpha s})^2} + 2s^2 e^{-\alpha s^2}, \tag{43}$$

which is what we wanted to show.
(ii) Consider γ_3, which comes from placing a hexagon near boundary type 3. We first visualise the possible placements in Fig. 9, where I and II correspond to two principally different positions of the placed hexagon, where the position of the hexagon is defined by the position of the upper left corner.

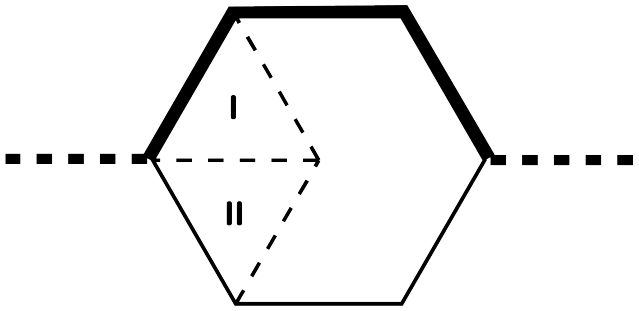

Figure 9: A boundary segment type 3, indicated by thick lines. The thick dashed lines show the continuation of the boundary. The two regions I and II are shown, which correspond to two principally different positions when the upper left corner of a hexagon is placed inside them.

We consider case I in Fig. 10. We can find that the uncoverable area here is

$$a = \frac{1}{2}x(x+2y+2s) + \frac{1}{2}(x+y)(s-x+s+y) + \frac{1}{2}y(2s-y) \tag{44}$$

$$= 2s(x+y) + xy \geq 2s(x+y). \tag{45}$$

For case II, the area is certainly larger than $2s^2$. When we do not place any hexagon, the area we obtain is certainly larger than $\frac{3}{2}s^2$. Again, we can then bound $\sum b$ as follows:

$$\sum_{j(i)} b_{j(i)} \leq \sum_{x=0}^{\infty}\sum_{y=0}^{\infty}\left(e^{-2\alpha s(x+y)}\right) + \frac{1}{2}s^2 e^{-2\alpha s^2} + e^{-\frac{3}{2}\alpha s^2} - 1, \tag{46}$$

where again we pick up a minus one because the case of $x = y = 0$ is not allowed. We can write the above as

$$\sum_{j(i)} b_{j(i)} \leq \frac{e^{-2\alpha s}(2-e^{-2\alpha s})}{(1-e^{-2\alpha s})^2} + 2s^2 e^{-2\alpha s^2} + e^{-\frac{3}{2}\alpha s^2}, \tag{47}$$

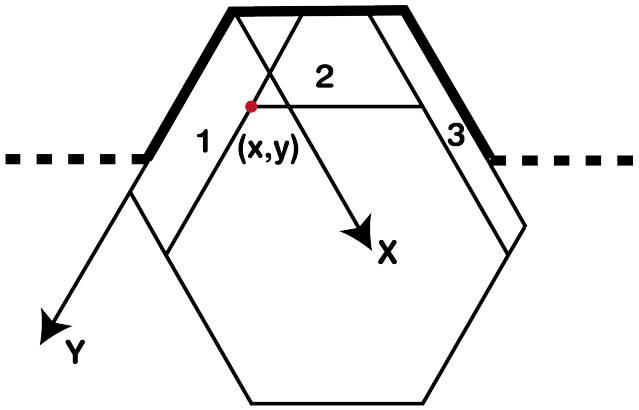

Figure 10: A boundary segment type 3 where the adjacent hexagon is in a position corresponding to case I. The uncoverable area is divided into three different regions.

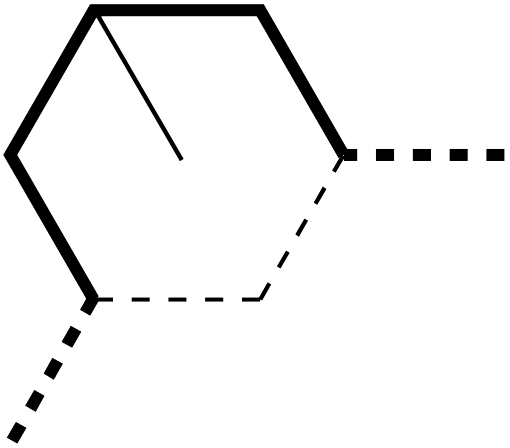

Figure 11: A boundary segment type 4, indicated by thick lines. The thick dashed lines show the continuation of the boundary. The hexagon will have the upper left corner on the thin line.

which is what we wanted to show.
(*iii*) Finally, let us consider γ_4. This is seen in Fig. 11, where the upper left point of the hexagon to be placed has to sit on the line in the figure.
An example is seen in Fig. 12. We then see the uncoverable area being

$$a = 2sx, \tag{48}$$

where we can then bound $\sum b$ by

$$\sum_{j(i)} b \leq \sum_{x=1}^{s} e^{-\alpha 2sx} \leq \frac{e^{-2\alpha s}}{1 - e^{-2\alpha s}}, \tag{49}$$

where we extended the sum to infinity. This is the expression we were looking for, proving (*iii*). This proves the lemma. ■

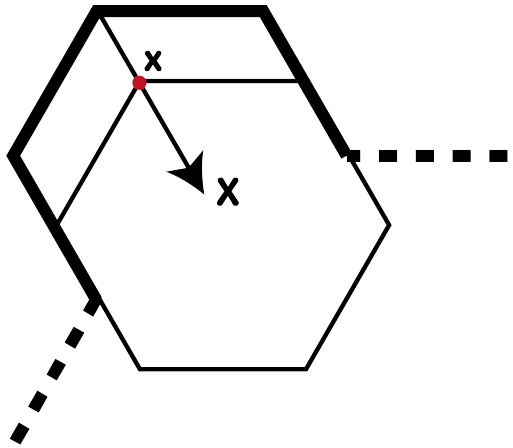

Figure 12: A hexagon placed next to boundary segment type 4.

We can find α_0 independent of s such that for $\alpha > \alpha_0/s$

$$\gamma_4 > \gamma_1^3 \tag{50}$$

and

$$\gamma_4 > \gamma_3^2. \tag{51}$$

We can then rewrite (35) by using (30), we can then see

$$S(B) \leq \gamma_1^{\eta(1)} \cdot \gamma_3^{\eta(3)} \cdot \gamma_4^{\eta(4)} \leq \gamma_4^{l/4}. \tag{52}$$

Now using the upper bound on the possible boundaries of length l containing a fixed hexagon x found in Lemma 1.2 (31) and the above (52), we find that

$$\tilde{p}(x) \leq \sum_{l=12}^{\infty} \frac{3}{4}\left(\frac{1}{48}l + \frac{1}{4l}\right) 2^l \gamma_4^{l/4} \tag{53}$$

$$= \sum_{i=6}^{\infty} \frac{3}{4}\left(\frac{1}{24}i + \frac{1}{8i}\right) (16\gamma_4)^{i/2} \tag{54}$$

$$= \frac{1}{32}\sum_{i=6}^{\infty}(i + \frac{3}{i})(16\gamma_4)^{i/2}. \tag{55}$$

We notice that the term with $\frac{3}{i}$ is very small compared to the term with i, so we can disregard it and look at the term with i instead. As

$$\sum_{i=6}^{\infty}(4\gamma_4^{1/2})^i = \sum_{i=0}(4\gamma_4^{1/2})^i \cdot (4\gamma_4^{1/2})^6 = \frac{(16\gamma_4)^3}{1-(4\gamma_4^{1/2})}, \tag{56}$$

and so

$$\sum_{i=6}^{\infty} i \cdot (4\gamma_4^{1/2})^i \leq \sum_{i=0} i \cdot (4\gamma_4^{1/2})^i \cdot (4\gamma_4^{1/2})^5 = \sum_{i=0} \partial_{4\gamma_4^{1/2}}(4\gamma_4^{1/2})^i \cdot (16\gamma_4)^3 = \frac{(16\gamma_4)^3}{(1-4\gamma_4^{1/2})^2}. \tag{57}$$

Using this in (55), we get

$$\tilde{p}(x) \leq C \cdot \frac{(16\gamma_4)^3}{(1-4\gamma_4^{1/2})^2} \tag{58}$$

where C is a constant, and provided that $\alpha > \alpha_0/s$ and $\delta \leq 1$.
For $s > 1$, we can find a positive constant ω_0 such that $\delta \leq 1$ provided that

$$\beta\mu = 3s^2\alpha \geq \omega_0 s \log s \tag{59}$$

Substituting this into (38), we find that

$$\gamma_4 = \frac{e^{-2\alpha s}}{1-e^{-2\alpha s}} \leq \frac{s^{-\frac{2}{3}\omega_0}}{1-s^{-\frac{2}{3}\omega_0}}, \tag{60}$$

so we get (using (58))

$$\tilde{p}(x) \leq C \cdot \frac{\dfrac{s^{-2\omega_0}}{(1-s^{-2\omega_0/3})^3}}{\left(1-4\cdot\left(\dfrac{s^{-2\omega_0/3}}{1-s^{-2\omega_0/3}}\right)^{1/2}\right)^2}, \tag{61}$$

which we can write as

$$\tilde{p}(x) \leq C s^{-2\omega_0} T, \tag{62}$$

where T is the term corresponding to the rest of the fraction, and goes to 0 for $s \to \infty$. We can thus bound T by some constant depending on ω_0. Taking both C and this constant together, we call it ω, such that

$$\tilde{p}(x) \leq \omega s^{-2\omega_0}, \tag{63}$$

which gives us our final bound for $\tilde{p}(x)$.
Let us now consider the second probability in (8), related to x being covered by a virtual hexagon that belongs to the boundary structure A. As we are in the grand canonical system, the probability of this is obviously

$$p_v(x) < e^{-\beta\mu}, \tag{64}$$

where we can again use (59) to find

$$p_v(x) < s^{-\omega_0 s}. \tag{65}$$

Now combining these two into

$$p_A(x) \leq \tilde{p}(x) + p_v(x), \tag{66}$$

we get

$$p_A(x) \leq \omega s^{-2\omega_0} + s^{-s\omega_0}. \tag{67}$$

where $s \geq 2$, so $s^{-s\omega_0} \geq s^{-2\omega_0}$. To get the above expression smaller than $1 - 1/3s^2$, we see that we would need

$$\frac{\omega + 1}{s^{2\omega_0}} \leq 1 - \frac{1}{3s^2} = \frac{3s^2 - 1}{3s^2}, \tag{68}$$

$$\frac{3(\omega + 1)}{3s^{2\omega_0}} \leq \frac{3s^2 - 1}{3s^2}, \tag{69}$$

$$\frac{3(\omega + 1)}{s^{\omega_0}} \leq 3s^2 - 1, \tag{70}$$

$$s^{\omega_0} \geq \frac{3(\omega + 1)}{3s^2 - 1}, \tag{71}$$

where $s \geq 2$, and ω is constant, so by choosing ω_0 large enough we can easily make sure the above holds. We then indeed get that

$$p_A(x) \leq 1 - \frac{1}{3s^2}, \tag{72}$$

2 Granular Hexagon Model

As noted in the introduction, the granular model we will be considering is an adaptation of the hard hexagon model described in the previous section, with added constraints as to mimic gravity and friction between the particles. As such, we again consider an infinite triangular lattice Λ, where hard-core regular hexagons are centred on the lattice. The side-length is a fixed integer multiple of the lattice length, and we call this integer s. We count the lattice points inside a hexagon the same way as before, giving us $M = 3s^2$ distinct lattice points, which correspond to the possible distinct tilings of the lattice. The hexagons are inside a container $V \subseteq \Lambda$, where the hexagons outside of V are tiling the lattice, i.e. they are of the same structure, which we will call the boundary structure A. The area not covered by hexagons in V we will call $V_{\text{no hex}}$. Same as before, we find ourselves in the grand canonical ensemble, and we define our grand canonical probability measure on the subsets of the set of all possible configurations as before, so for a fixed volume V our $m_v(\mu)$ is defined as in (5), and m is the weak limit.
To make this model a toy model for granular matter, we introduce the following constraint:

Constraint 2.1. *For all hexagons inside V, at least one of their lower three edges must intersect at least one of the three upper edges of another hexagon.*

This means that we are restricting the phase space only to the configurations which are stable under the combined effects of gravity and infinite friction, which are what the Edwards' approach for modelling granularity requires [EO89]. An important fact to immediately notice with our knowledge of the Peierls' argument and contours is that this constraint restricts the possible contours. Where before we could have a hexagon or a region of hexagons that was completely on its own, meaning it is not touching any other hexagon, now we cannot have this any longer, restricting the possibilities of configurations inside a contour. A simple example signifying what can and cannot be encountered is seen in Fig. 13.
Apart from this, our discussion of contours and distinct structures will be similar to the non-granular case, where we have M different possible states and $\dfrac{M(M-1)}{2}$ different types of Peierls' contours. As such, most of what will follows will mirror the text on the non-granular hexagon model, and we will take special notice of anything that does change. Immediately, there is a point to be made about placement of the virtual hexagons: if there is a void in a configuration that is large enough to house an additional hexagon, we will fill the void by placing a virtual hexagon conform the constraints, that is, having at least one of the lower three edges of the virtual hexagon intersect with one of the upper three edges of another hexagon, real or virtual. If a void is big enough to house multiple virtual hexagons, we place them down to up, such that the constraint is always adhered to.
We now define the following terms, and we note that these definitions are the same in the non-granular hexagon model.

Definition 2.1. *We define the edge set E as*

$E := \{\lambda \in \Lambda : \lambda$ *is a shared part of two hexagons belonging to different tilings (structures)*$\}$.

Using this and $V_{\text{no hex}}$, we define the following:

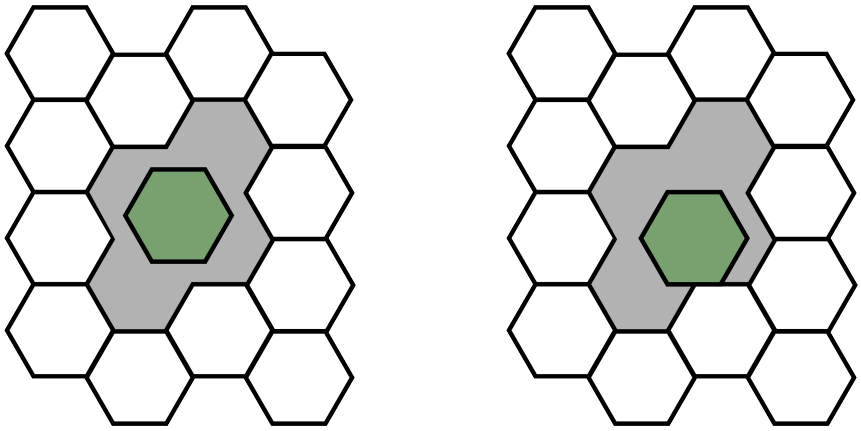

(a) Configuration 1 (b) Configuration 2

Figure 13: Two examples of hard hexagon configurations, where the white hexagons are boundary hexagons surrounding V, and the green hexagon is the only hexagon inside V. The configuration on the left is not allowed in the granular hard hexagon model, but is allowed in the non-granular case, as the green hexagon does not have a lower edge which intersects with another hexagon. The configuration on the right is allowed in both models

Definition 2.2. *A contour C is a connected component of the set of all elements of contour, where an element of contour is an element of the set*

$$\overline{V_{no\ hex}} \cup E,$$

meaning that an element of contour is either a lattice point not covered by a hexagon or the lattice point is shared by two hexagons of different tiling/structure.

We again note that this allows for contours inside other contours.

Definition 2.3. *The area $A(C)$ of a contour C equals one-half the number of elementary triangles constituting the empty area of the contour.*

Our boundary and its structure are fixed, and we will call the boundary structure A. Again we can note that a point inside the boundary that is not covered by a hexagon of the A structure must be surrounded by a contour, or must be part of the contour itself. We only have to consider outer contours, as they will be surrounded by the A structure. We specify a contour in the model as follows: imagine a place of hexagons of the boundary structure A, then the edges of the hexagons create a hexagonal lattice. We can now create a hole in this structure, where the hole is a self-avoiding polygon on this hexagonal lattice. The polygon, called B, constitutes the boundary between the outer A structure and the contour. We then describe the positions of all the hexagons next to the boundaries of the hole. These hexagons are positioned in accordance to the position constraints. With this, we have specified the outer boundary between A and the contour, and the inner boundaries between the contour and the different structures which are found inside.
A contour C splits the interior hexagons into different regions which are separated from the boundary structure A, and from each other. These regions are called C-interior regions, and

note that the region of hexagons that are positioned adjacent to C will all have the same structure, which we will call the boundary structure of the region.

Our discussion on use of the Peierls' argument in this model is similar to the non-granular case; we do not discuss working with M different substructures again. There is a point to be made on the deletion of terms in the partition function, however. We repeat (6) here

$$p(C) = \frac{\sum_{\omega:\omega\ni C} w(\omega)}{\sum_{\omega} w(\omega)}, \tag{73}$$

with $w(\omega)$ the canonical weight of a configuration ω and the denominator of the expression above is the total partition function. The general argument of why we can delete terms in the partition function to get a one-to-one relationship between the terms in the numerator and denominator will be the same. However, it hinges on the possibility of transforming a configuration with C to one without C by removing some elements and reflecting the rest. As our configurations are now constrained in some way, we should think about whether this process, outlined in the section on the non-granular hexagon model, is still valid. First of all, any configuration we find in the sum in the denominator is allowed by our constraint by definition of the partition function. We can then follow the reflection/deletion process, resulting in a configuration where C is deleted and we can place $A(C)/M$ new hexagons to fill up the area. If this configuration is not allowed according to our constraints, we can then take every C-interior region (that now is not C-interior anymore as C has been deleted), and translate it such that they are all of the A-structure. This can be done as the centre of every hexagon is situated in a hexagon-sized area around every A-structure lattice point in Λ. After this, we can fill up the area of the deleted contour with $A(C)/M$ new hexagons, meaning that again, every hexagon inside the configuration has one of the lower three edges supported by another hexagon. It should be noted that before, placing $A(C)/M$ hexagons was used as an upper bound, meaning we didn't need to place all of the $A(C)/M$ hexagons. Now, to ensure that the configuration is allowed by our constraints, we have to place all $A(C)/M$ hexagons. We then have a term in the denominator having a one-to-one relation with a term in the numerator, where both configurations are allowed by our constraints. With this, we have taken care of the deletion of terms in the partition function, and we can continue using the Peierls' argument.

We define the probability of belonging to the A-structure:

Definition 2.4. *The probability $p_A(x)$ for a given point $x \in L$ gives the probability that the point x is not covered by a hexagon belonging to the A structure.*

We again pose the theorem:

Theorem 2.1. *For the granular hard hexagon model, for sufficiently large activity z, and x a point on the lattice, we have that $1 - p_A(x) > (3s^2)^{-1}$, that is, a hexagon covering x will not be centred equiprobably on each of the $3s^2$ sublattices.*

Again, this means that for a large enough activity z the boundary influences the positions of the hexagons, and thus This means that for a large enough activity z, the boundary starts influencing the positions of the hexagons in the system. This implies the following corollary:

Corollary 2.1. *There exists an order-disorder phase transition in the granular hard hexagon model.*

This is in agreement with our hypothesis that for small z, the model is in a disordered state, and for large enough z it is in an ordered state. We will provide the argument for a small z resulting in a disordered state in the next chapter on the Monte-Carlo simulation.

2.1 Proof Theorem 2.1

Mirroring our proof of Theorem 1.1, there are three possibilities of a lattice point x not being covered by a hexagon belonging to the A-structure: there is no hexagon covering x, the hexagon covering x belongs to a different structure, or x is covered by a virtual hexagon of structure A. This means that x is part of a contour or surrounded by a contour. We can upper bound our probability $p_A(x)$ by the probability that x is surrounded by or part of a contour C, plus the probability that x belongs to a virtual hexagon of the A-structure. We define:

Definition 2.5. *The probability $\tilde{p}(x)$ for a given point $x \in L$ gives the probability that point x is either surrounded by a contour or part of a contour.*

Definition 2.6. *The probability $p_v(x)$ for a given point $x \in L$ gives the probability that point x is covered by a virtual hexagon that belongs to the boundary structure A.*

We write

$$p_A(x) \leq \tilde{p}(x) + p_v(x). \tag{74}$$

We first focus on the probability that a point x is surrounded by or part of a contour. We know

$$Z = \sum_i e^{n_i \mu \beta}, \tag{75}$$

where i sums over all possible individual configurations, with n_i particles. The probability is of certain configuration j appearing is then

$$p(\text{configuration } j) = \frac{e^{n_j \mu \beta}}{Z}. \tag{76}$$

The probability of outer contour C is given by

$$p(C) = \sum_{i : i \ni C} \frac{e^{n_i \mu \beta}}{Z}, \tag{77}$$

where we sum over all the configurations that contain C as outer contour. We can upper bound this by deletion of terms in the partition function. This is similar to the non-granular model, and we discussed any possible problems earlier this chapter. We then get

$$p(C) \leq \frac{\sum_{i : i \ni C} e^{n_i \mu \beta}}{\sum_{i : i \ni C} e^{(n_i + A(C)/M)\mu \beta}} = e^{-A(C)\mu\beta/M}, \tag{78}$$

as upper bound for the probability $p(C)$, with $A(C)$ the area of contour C. We then write

$$\tilde{p}(x) = \sum_{C:C\ni x} p(C), \tag{79}$$

where the sum runs over all C such that x is inside the outer boundary B of C. We can upper bound this by

$$\tilde{p}(x) = \sum_{C:C\ni x} e^{-A(C)\mu\beta/M}. \tag{80}$$

We make a distinction between outer boundaries and inner hexagons next to C, so we write

$$\tilde{p}(x) = \sum_{B:B\ni x} S(B), \tag{81}$$

where we sum over all outer boundaries B with the property that point x is inside of B, and where

$$S(B) = \sum_{\text{inner hex}} e^{-A(C)\mu\beta/M}, \tag{82}$$

where we sum over all the inner hexagons next to C. As before, we split this $S(B)$ as a summation over outer inner hexagons and inner inner hexagons:

$$S(B) = \sum_{\substack{\text{outer}\\ \text{inner}\\ \text{hexagons}}} \sum_{\substack{\text{inner}\\ \text{inner}\\ \text{hexagons}}} e^{-A(C)\mu\beta/M}. \tag{83}$$

The shape of B decides how many outer inner hexagons there are in a configuration. The maximal amount we will call n. The first sum in (83) will then be over the possible position coordinates of hexagons $1,\ldots,n$. We write the position coordinates as $j(1),\ldots,j(n)$. In similar fashion, the amount of inner inner hexagons is determined by the shape of B, and we denote the maximal amount of these hexagons as m. The second sum in (83) will then be over $j(n+1),\ldots,j(n+m)$. We then write

$$S(B) = \sum_{j(1)} \cdots \sum_{j(n+m)} e^{-A(C)\mu\beta/M}. \tag{84}$$

$A(C)$ depends on the shape of B and the position coordinates $j(1),\ldots,j(n+m)$. We want to divide the total $A(C)$ into contributions assigned to each of the $n+m$ hexagons inside B. Similar to the non-granular model, we look at hexagon-sized areas centred on the A lattice, where either one or no hexagon can be placed. For a given position of a placed hexagon, the uncoverable area is calculated as if no other hexagon is placed, and is the uncovered area in the respective hexagon-sized area plus any additional uncoverable area outside of it if it is certain that it cannot be made uncoverable by another hexagon. For the inner inner hexagons, we take a similar approach as we did before. Both of these will be worked out in much more detail later on, when we find upper bounds for the position sums. We then write

$$A(C) = \sum_{i=1}^{n+m} a_i, \tag{85}$$

where a_i is the contribution of hexagon i to $A(C)$. Under the area-contribution rules, a_k is independent of the position $j(l)$ for each hexagon $l > k$. Then, introducing

$$b_{j(i)} = e^{-a_i \mu M \beta}, \tag{86}$$

we can rewrite $S(B)$ and (18) as follows:

$$S(B) = \sum_{j(1)} b_{j(1)} \cdots \sum_{j(n+m)} b_{j(n+m)}. \tag{87}$$

Again, for any hexagon i we cannot place, we get $a_i = 0$ and thus $\sum_{j(i)} b_{j(i)} = 1$.
We will now upper bound $\sum_{j(i)} b_{j(i)}$ for $i > n$.

Lemma 2.1. *We can bound* $\sum_{j(i)} b_{j(i)} \leq \max\{\delta'(\mu M \beta, s), 1\}$ *for* $i > n$*, where* δ' *is independent of the fixed values of the positions of the preceding hexagons* $j(1), \ldots, j(i-1)$*.*

Proof Lemma: Within the sum over the inner inner hexagons, we place hexagons in a fixed order s.t. we enlarge the uncoverable area as much as possible. We do this via a stepwise placement method, creating C. The area-contribution rules give us that the area contributed to a hexagon depends on the position of it relative to two preceding hexagons. In Fig. 14 we see the possible placement of the second hexagon, where the position of the second hexagon is given by the position of its lower right corner (the perspective is flipped as opposed to the non-granular model to make clear that we follow the constraints in our examples/calculations). The possibilities for placement are very restricted, as we have to keep in mind we work under granularity constraints.

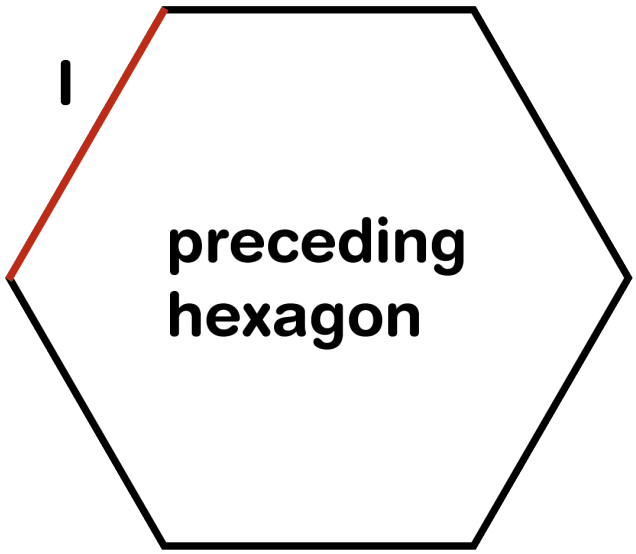

Figure 14: The possible placement of the second hexagon, where the lower right corner has to be on the red line to fulfil granularity constraints.

For placing the third hexagon, we get a couple of principally different positions, as we can see in Fig. 15. The v signifies the relative position of the two preceding hexagons compared

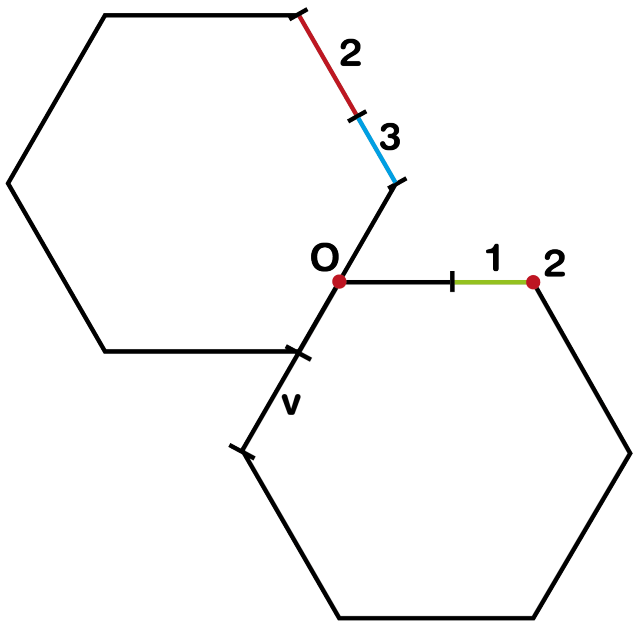

Figure 15: The two preceding hexagons are placed in one of the allowed positions. We define the relative position with coordinate v. The numbered regions correspond to different positions of the next hexagon, provided that the position is defined by the position of the lower left corner. Placing the lower left corner on the green line (numbered 1) leads to the same bound on the area, placing it on the red line and dot (numbered 2) lead to another bound, and placing it on the blue line (numbered 3) leads it to yet another bound.

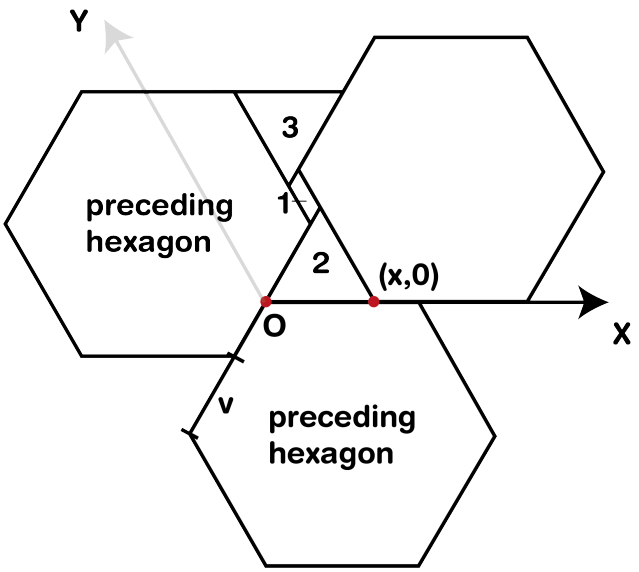

Figure 16: The two preceding hexagons are placed in allowed positions, and the next hexagon is placed in position 1 as seen in Fig. 15. The position of the third hexagon, marked by position of the lower left corner of the hexagon is given by coordinates x, y. The uncoverable area is divided in three numbered regions.

to each other. There are three distinct possibilities for placing the third hexagon, which are numbered $1-3$ in the figure.
Consider a hexagon placed in a position 1, as seen in Fig. 16. This third hexagon brings two additional coordinates x, y that signify its relative position towards the origin. We can calculate the uncoverable by using these coordinates. We can split the uncoverable area into different subareas, as seen in Fig. 16. This gives us the following area:

$$a = (x - v)(s - x) + \frac{1}{2}x^2 + \frac{1}{2}x^2 \tag{88}$$

$$= x^2 - x^2 + x(v + s) - vs = x(v + s) - vs. \tag{89}$$

For hexagons in position 2, seen in Fig. 17, we find that we always have that

$$a \geq \frac{1}{2}s^2, \tag{90}$$

as we can always place at least one triangle with side s in the uncoverable area.
The total number of positions leading to position 2 is always less or equal to $s + 1$.
For hexagons in position 3, seen in Fig. 18, we again split up the area in three regions. We use the additional coordinates x, y to calculate the following area:

$$a = y(s - y + v) + \frac{1}{2}(y - v)^2 + \frac{1}{2}(y - v)^2 \tag{91}$$

$$= y^2 - y^2 - 2yv + v^2 + sy + yv = v^2 + y(s - v). \tag{92}$$

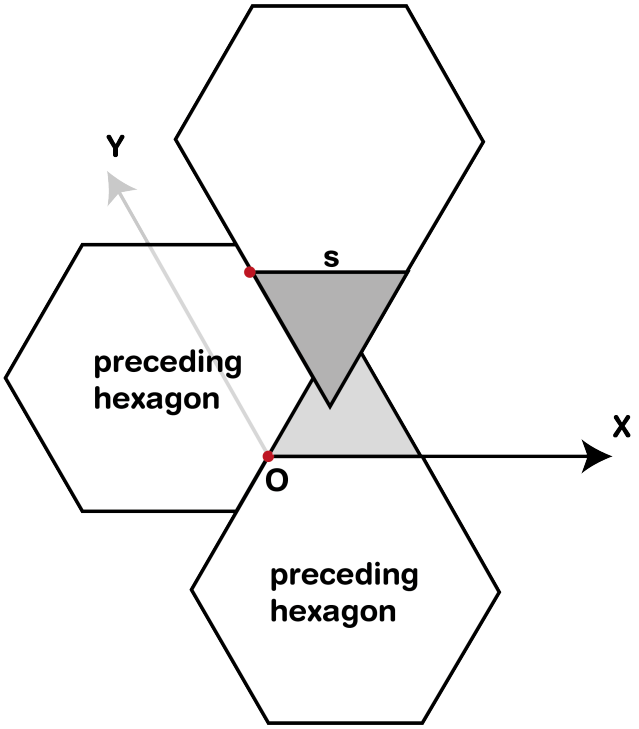

Figure 17: The preceding hexagons in allowed position and the third hexagon placed in position 2 as in Fig. 15. The uncoverable area (shaded) exceeds $\frac{1}{2}s^2$.

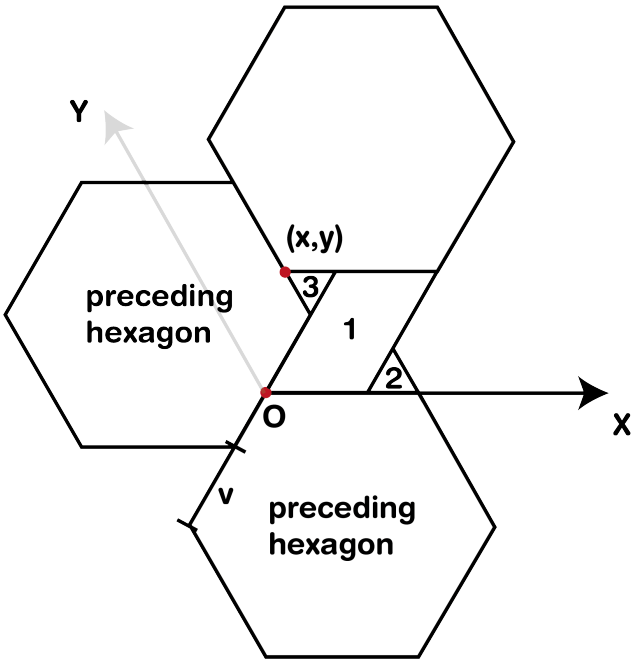

Figure 18: The preceding hexagons in allowed position and the third hexagon placed in position 3 as in Fig. 15. The uncoverable area is split up in three numbered regions.

As we discussed the possible positions and their respective uncoverable area contribution, we can sum them all together and extend the upper limit to infinity to upper bound $\sum b$:

$$\sum_{j(i)} b_{j(i)} \leq \sum_{x=1}^{\infty} \left(e^{-\alpha(x(v+s)} e^{-\alpha vs}\right) \sum_{y=1}^{\infty} \left(e^{-\frac{\alpha}{2}v^2} e^{-\alpha y(s-v)}\right) + (s+1)e^{-\frac{\alpha}{2}s^2} \tag{93}$$

$$= \left(e^{-\alpha vs} e^{-\frac{\alpha}{2}(v^2)} (1-e^{-\alpha(s-v)})^{-1} (1-e^{-\alpha(s+v)})^{-1}\right) + (s+1)e^{-\frac{\alpha}{2}s^2} \tag{94}$$

$$\tag{95}$$

where $\alpha = \frac{\mu}{MkT} = \frac{\mu}{3s^2kT}$. As $v \in \{0, \ldots, s-1\}$ for the first terms, we can bound this by:

$$\sum_{j(i)} b_{j(i)} \leq \left(e^{-\alpha(s+\frac{1}{2})} (1-e^{-\alpha(s)})^{-1} (1-e^{-\alpha(s-(s-1))})^{-1}\right) + (s+1)e^{-\frac{\alpha}{2}s^2} \equiv \delta', \tag{96}$$

This final expression is what we call δ'.
As stated before, when a hexagon can't be placed, a_k becomes 0 which corresponds to $\sum_{j(k)} b_{j(k)} = 1$, hence we can upper-bound $\sum_{j(i)} b_{j(i)} \leq \max\{\delta(\beta\mu/M, s), 1\}$, proving the lemma. ■

Using (87) and Lemma 2.1, we can find that

$$S(B) \leq 1 \cdot \sum_{j(1)} b_{j(1)} \cdots \sum_{j(n)} b_{j(n)}, \tag{97}$$

provided that $\delta \leq 1$. We effectively upper-bounded $S(B)$ with the positions of only the outer inner hexagons. We need an expression for the sum over all B containing x, and we need to find an expression for the sums over the position of outer inner hexagons. The placement of these hexagons depends directly on the shape of B. As from before, we know that B must be made up out of five different types of boundary segments, which are in Fig. 6. The same discussion as for the non-granular case applies here: type 5 cannot show up, we call l the length of B in units of hexagon and we let $\eta(i)$ the number of segments of type i in a boundary. We repeat (30)

$$l = 2\eta(1) + \eta(2) + 3\eta(3) + 4\eta(4). \tag{98}$$

We can use the same upper bound for the amount of boundaries B containing point x as in the non-granular case (Lemma 1.2), so I will only repeat the statement:

Lemma 2.2. *The number of boundaries B with a given length l surrounding a fixed hexagon ν is less than $\nu(l)$, where*

$$\nu(l) = \left(\frac{3 \cdot 2^{l-2}}{l}\right)\left(\frac{1}{48}l^2 + \frac{1}{4}\right). \tag{99}$$

Again, we can place one outer inner hexagon next to each segment, with the note that a hexagon next to segment type 2 is regarded as an inner inner hexagon. We can then write the bound

$$\sum_{j(i)} b_{j(i)} \leq \gamma_k(\beta\mu/M, s), \quad i \leq n, \tag{100}$$

where k refers to the type of the segment to which the ith hexagon is located.

Lemma 2.3. *The γ_k bounds are as follows:*

$$(i) \quad \gamma_1 = \frac{e^{-\alpha s}}{(1 - e^{-\alpha s})} \tag{101}$$

$$(ii) \quad \gamma_3 = \frac{e^{-2\alpha s}}{1 - e^{-2\alpha s}} \tag{102}$$

$$(iii) \quad \gamma_4 = \frac{e^{-2\alpha s}}{1 - e^{-2\alpha s}}, \tag{103}$$

Proof Lemma: (i) Let us start by considering γ_1, so placing a hexagon near boundary type 1, as seen in Fig. 6. We can visualise the possible placements as in Fig. 19, where we have two red lines signifying placing a hexagon there results in a different shape of the uncoverable area, provided that the position of the placed hexagon is given by the position of the lower right corner. In reality, both cases are equivalent to each other via symmetry, so we only need to consider one of the two.

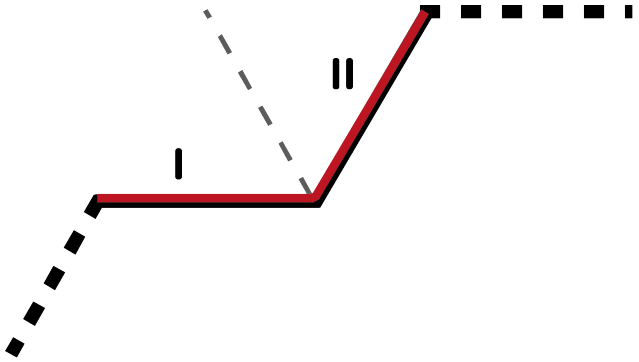

Figure 19: A segment of type 1, denoted by thick lines. The thick dashed lines show the continuation of the boundary. The two regions I and II correspond to the two principally different positions the hexagon can be in, depending on where the lower right corner of the adjacent hexagon is placed.

Let us consider a hexagon in situation II, this is seen in Fig. 20. We see that the uncoverable area we find is a single region, giving us

$$a = ys. \tag{104}$$

We can then upper bound the sum by

$$\sum_{j(i)} b_{j(i)} \leq \sum_{y=1}^{s} \left(e^{-\alpha s y}\right) - 1, \tag{105}$$

where we pick up the minus one from the fact that the position $x = y = 0$ is not allowed, as this would mean that the hexagon is of the A-structure. We can remove the sum by letting

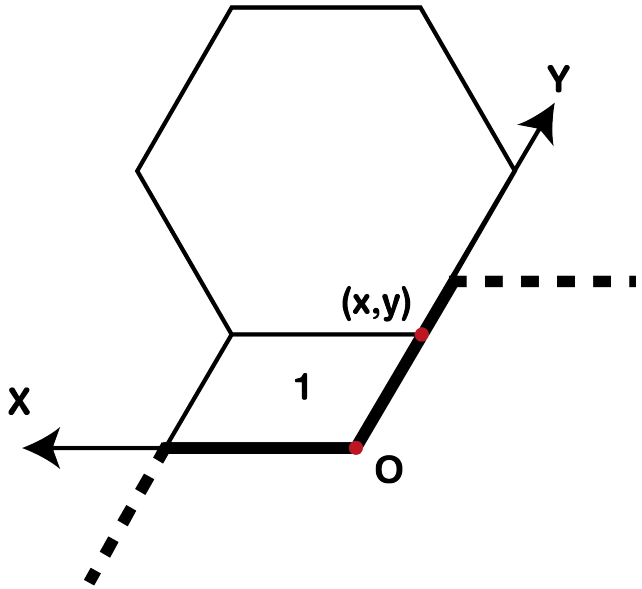

Figure 20: A segment of type 1 and the placed hexagon in a case II position. The relative position of the hexagon is denoted by the coordinates x and y.

it go to infinity and then

$$\sum_{j(i)} b_{j(i)} \leq \frac{1}{(1-e^{-\alpha s})} - 1 \tag{106}$$

$$= \frac{e^{-\alpha s}}{(1-e^{-\alpha s})}, \tag{107}$$

which is what we wanted to show.

(*ii*) We consider γ_3. There really is one type of position as well for this boundary segment, visualised by the two red lines in Fig. 21. Again the position of the hexagon is defined by the position of the bottom right corner.

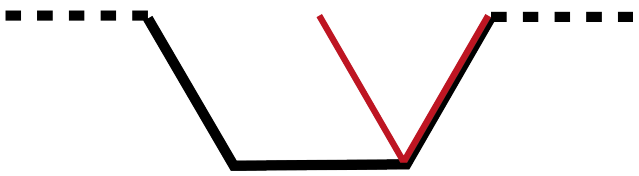

Figure 21: A boundary segment type 3, indicated by thick lines. The thick dashed lines show the continuation of the boundary. The red line shows the possible positions of the lower right corner of the hexagon to be placed.

We consider a case in Fig. 22. We can find that the uncoverable area here is

$$a = \frac{1}{2}y^2 + sy + y(s-y) + \frac{1}{2}y^2 - 1 \tag{108}$$

$$= 2sy - 1, \tag{109}$$

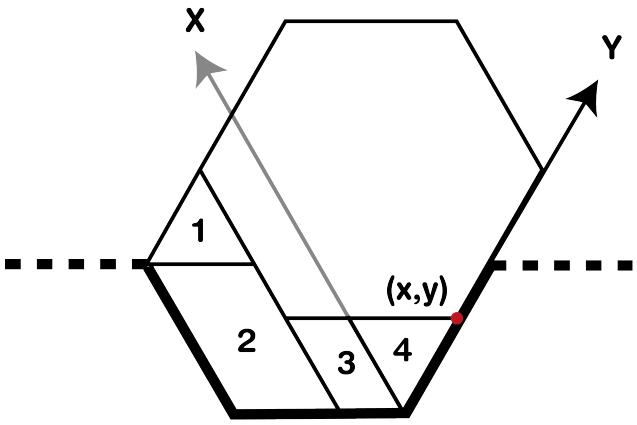

Figure 22: A boundary segment type 3, and a placed hexagon. The relative position of the hexagon is denoted with two coordinates x, y. The uncoverable area is split up into four regions.

where again the minus is for not allowing the case $x = y = 0$. We can then get the bound

$$\sum_{j(i)} b_{j(i)} \leq \sum_{y=0}^{\infty} e^{-2\alpha s y} - 1, \tag{110}$$

$$= \frac{e^{-2\alpha s}}{1 - e^{-2\alpha s}}, \tag{111}$$

which is what we wanted to show.
(*iii*) Finally, let us consider γ_4. As this case does not change at all compared to the non-granular model, we will not prove this again here. Combining the above, this proves the lemma. ■

We can find α_0' independent of s such that for $\alpha' > \alpha_0'/s$

$$\gamma_4 > \gamma_1^3 \tag{112}$$

and obviously

$$\gamma_4 > \gamma_3^2. \tag{113}$$

We can then rewrite (100) by using (98), we can then see

$$S(B) \leq \gamma_1^{\eta(1)} \cdot \gamma_3^{\eta(3)} \cdot \gamma_4^{\eta(4)} \leq \gamma_4^{l/4}. \tag{114}$$

Now we use the upper bound on amount of boundaries B of length l containing x found in Lemma 2.2 and the above to get

$$\tilde{p}(x) \leq \sum_{l=12}^{\infty} \frac{3}{4}\left(\frac{1}{48}l + \frac{1}{4l}\right) 2^l \gamma_4^{l/4} \tag{115}$$

$$= \sum_{i=6}^{\infty} \frac{3}{4}\left(\frac{1}{24}i + \frac{1}{8i}\right) (16\gamma_4)^{i/2} \tag{116}$$

$$= \frac{1}{32}\sum_{i=6}^{\infty}(i + \frac{3}{i})(16\gamma_4)^{i/2}. \tag{117}$$

where we used $2i = l$. Again, as the term $\frac{3}{i}$ will go to zero for $i \to \infty$, we disregard in comparison with the i term. As

$$\sum_{i=6}^{\infty}(4\gamma_4^{1/2})^i = \sum_{i=0}^{\infty}(4\gamma_4^{1/2})^i \cdot (4\gamma_4^{1/2})^6 = \frac{(16\gamma_4)^3}{1-(4\gamma_4^{1/2})}, \tag{118}$$

we get that

$$\sum_{i=6}^{\infty} i \cdot (4\gamma_4^{1/2})^i \leq \sum_{i=0} i \cdot (4\gamma_4^{1/2})^i \cdot (4\gamma_4^{1/2})^5 = \sum_{i=0} \partial_{4\gamma_4^{1/2}}(4\gamma_4^{1/2})^i \cdot (16\gamma_4)^3 = \frac{(16\gamma_4)^3}{(1-4\gamma_4^{1/2})^2}. \tag{119}$$

We use this in (117), and get

$$\tilde{p}(x) \leq C \cdot \frac{(16\gamma_4)^3}{(1-4\gamma_4^{1/2})^2} \tag{120}$$

where C is a constant, and provided that $\alpha > \alpha_0/s$ and $\delta \leq 1$.
For $s > 1$, we find a positive constant ω_0' s.t. $\delta' \leq 1$ provided that

$$\beta\mu = 3s^2\alpha \geq \omega_0' s \log s, \tag{121}$$

where we use a prime to distinguish it from the similar constant for the non-granular model. We use this in (103):

$$\gamma_4 = \frac{e^{-2\alpha s}}{1-e^{-2\alpha s}} \leq \frac{s^{-\frac{2}{3}\omega_0'}}{1-s^{-\frac{2}{3}\omega_0'}}. \tag{122}$$

Using (120)

$$\tilde{p}(x) \leq C \cdot \frac{\frac{s^{-2\omega_0'}}{(1-s^{-2\omega_0'/3})^3}}{\left(1-4\cdot\left(\frac{s^{-2\omega_0'/3}}{1-s^{-2\omega_0'/3}}\right)^{1/2}\right)^2}, \tag{123}$$

which we can write as

$$\tilde{p}(x) \leq C s^{-2\omega_0'} T, \tag{124}$$

where T is the term corresponding to the rest of the fraction, which goes to 0 for $s \to \infty$. We can thus bound T by some constant depending on ω_0', which we will call ω'. Then

$$\tilde{p}(x) \leq \omega' s^{-2\omega_0'}, \tag{125}$$

which gives us our final bound for $\tilde{p}(x)$.
We now consider the probability of x being covered by a virtual hexagon of structure A. Similar to the non-granular case, as we are in the grand-canonical ensemble, the probability of this is

$$p_v(x) < e^{-\beta\mu}, \tag{126}$$

where we can use (121) to find

$$p_v(x) < s^{-\omega_0' s}. \tag{127}$$

Combining the two probabilities, we find

$$p_A(x) \leq \omega' s^{-2\omega_0'} + s^{-s\omega_0'}, \tag{128}$$

where we can choose ω_0' small enough (similar to in the non-granular case) to get

$$p_A(x) \leq 1 - \frac{1}{3s^2}, \tag{129}$$

which is what we needed to show. ■

3 Simulation

As stated before, granular matter does not exist at very low densities, and that means we cannot use the statistical mechanics argument telling us that at low densities -as the particles are essentially independent- the particles are insensitive to the boundary. We provide an argument for a disordered phase at low density (low μ) in the form of a Markov chain Monte Carlo simulation on the model for a range of values of μ. We first quickly discuss Monte Carlo simulations as a whole, and provide our error analyses, and then provide our findings.

3.1 Monte Carlo Simulation

Monte Carlo methods are incredibly useful for simulating complex systems with many degrees of freedom. We will be using the Metropolis algorithm, which works as follows.

We write Ω for the finite set of all configurations of the system. Then we let

$$\mathbb{P}(\omega) = f(\omega)/Z, \tag{130}$$

be the probability of $\omega \in X$, with $f : X \to \mathbb{R}$ a known function and $Z = \sum_{\omega \in X} f(\omega)$ the normalisation.

The Metropolis algorithm generates a sequence of configurations $(\omega_n)_n$, where ω_k is the kth configuration. Every Monte Carlo step it generates a new configuration ω_{k+1} based on the current configuration ω_k according to a set of rules. If ω_k is selected, a trial configuration ω_k' is proposed by the algorithm, where then the probability of ω_k' relative to ω_k is

$$\frac{\mathbb{P}(\omega_k')}{\mathbb{P}(\omega_k)} = \frac{f(\omega_k')}{f(\omega_k)}, \tag{131}$$

where we note that the (often hard to compute) normalisation Z has disappeared from the equation. We let

$$p := \min\{1, \mathbb{P}(\omega_k')/\mathbb{P}(\omega_k)\}, \tag{132}$$

and then set $\omega_{k+1} = \omega_k'$ with probability p, and $\omega_{k+1} = \omega_k$ with probability $1 - p$.

Let us now consider a sequence $(\omega_n)_n$, where ω_0 is the starting configuration. If

1. for all $\omega, \omega' \in X$, $\mathbb{P}(\omega \to \omega')\mathbb{P}(\omega) = \mathbb{P}(\omega' \to \omega)\mathbb{P}(\omega')$;

2. any configuration ω can be reached with positive probability from starting configuration ω_0; and

3. f is not a constant function,

then it can be proven that, if we let $n \to \infty$, the selection of configurations follow (130), independent of which starting configurations ω_0 is used.

3.2 Specifics of Simulation

Let us now talk a bit more about the specifics of our simulation of the granular hard hexagon model. As stated before, the main goal of the simulation is to find a low-density counterpart to Theorem 2.1, which we will state as the following:

Conjecture 3.1. *For the granular hard hexagon model, for sufficiently small activity z, and x a point on the lattice, we have that $1 - p_A(x) = (3s^2)^{-1}$, that is, a hexagon covering x will be centred equiprobably on each of the $3s^2$ sublattices.*

This would signify a disordered state in the low density case of the granular hexagon model. For the simulation, we focus specifically on x being a point in the middle of the lattice that is of the boundary sublattice.
As stated above, we have a basic algorithm that tells us how to get a new configuration from a previous one. This works as follows: There are three possible actions that can happen in a single MC step, namely adding a hexagon, removing a hexagon and moving a hexagon. The first two are grouped together, as they both are an exchange with an outside hexagon reservoir.
The algorithm starts by either exchanging with the reservoir, or moving a hexagon in the system, both with probability $p = 0.5$. As there are six directions we can move a hexagon in, we uniformly ascribe $p = 1/6$ to each of the directions. For the exchange with the reservoir, we choose to either add or remove a hexagon with a probability $p = 0.5$, and we add a particle with probability $p = e^{-\mu}$ and remove a particle with probability $p = 1$. It is easily checked that the algorithm makes for a reversible, aperiodic Markov chain.
We introduce the following two functions:

$$\delta(\omega) := \begin{cases} 1, \text{if } \omega \text{ contains a hexagon centred at } x \\ 0, \text{otherwise} \end{cases} \tag{133}$$

$$t(\omega) := \begin{cases} 1, \text{if } \omega \text{ contains a hexagon centred at a point inside a hexagon centred at } x \\ 0, \text{otherwise} \end{cases} \tag{134}$$

(135)

As we are interested in the term $1 - p_A(x)$, which we cannot find analytically this time, we compute a statistic with the expected value of $1 - p_A(x)$, namely

$$p_M := \frac{\delta(\omega_1) + \delta(\omega_2) + \cdots + \delta(\omega_M)}{t(\omega_1) + t(\omega_2) + \cdots + t(\omega_M)}, \tag{136}$$

where M is the amount of steps we consider and $t(\omega), \delta(\omega)$ as above. The expected value of p_M is exactly $1 - p_A(x)$.

For the simulation, we work with a system of volume 784 hexagons, which corresponds to a 28x28 volume enclosed by a boundary (making the entire system including boundary 30x30 hexagons). The hexagon radius $s = 3$, which according to our conjecture tells us we expect $p_M \to 1/27$. We simulate for μ in a range between 0.1 and 10.0 -similar to [AR11]- where the

values of μ between 0.1 and 2 are of step size of 0.1, and the values between 2 and 10 are of step size 0.5. The bigger range of μ is chosen as we expect to see the phase transition in the model around there, similar to in [AR10]. To make sure that we simulate for a large enough amount of steps for the samples to be accurate, we calculate the autocorrelation, given by

$$R(k) = \frac{\sum_{i=0}^{n-k}(\psi(\omega_i) - \lambda) \cdot (\psi(\omega_{i+k}) - \lambda)}{(n-k+1)\sigma^2}, \tag{137}$$

where $\psi(\omega)$ is the volume fraction, λ the average of ψ over $\omega_1, \ldots \omega_n$ and σ^2 the variance. The autocorrelation for a typical simulation can be seen in Fig. 25

The starting configuration (which is empty) and a typical ending configuration (where $\mu = 2.0$) can be seen in Fig. 23 and 24. We see the autocorrelation function for our simulations

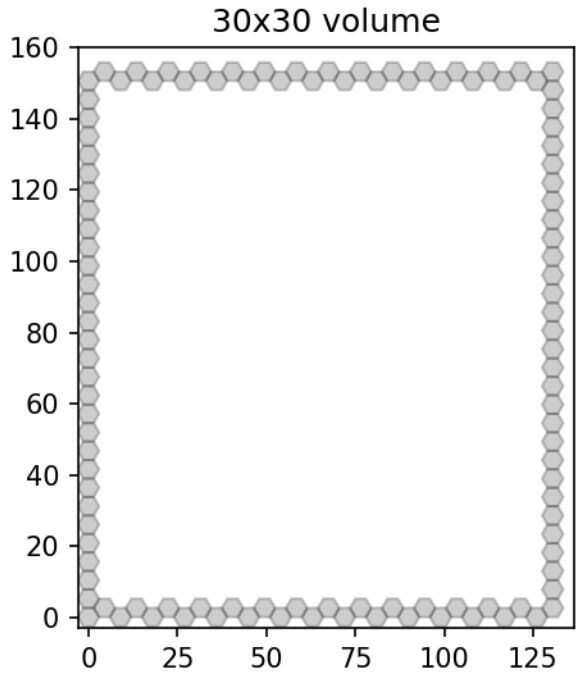

Figure 23: The starting configuration (an empty volume).

plotted in Fig. 25. We can see that after ten million steps on, the autocorrelation function is already in a tight band around zero. We let every simulation run for 400 million steps, to minimise the effect of irregularities on p_M. The simulations ran on the ITP Gemini cluster server.

We see the $p_M(\mu)$ for μ between 0 and 2 in Fig. 26. The complete simulated range of μ is seen in Fig. 27 . In both graphs, the red line is the expected value of $p_M = 1/27 = 1/(3 \cdot 3^2)$, as according to the conjecture with $s = 3$. We see that the simulated values are very much in line with our theory, thus supporting our main conjecture. We note that we did not see a phase transition in the range of $\mu \in (2, 10)$, which is opposite of what we expected from [AR10]. More on this will be in the discussion.

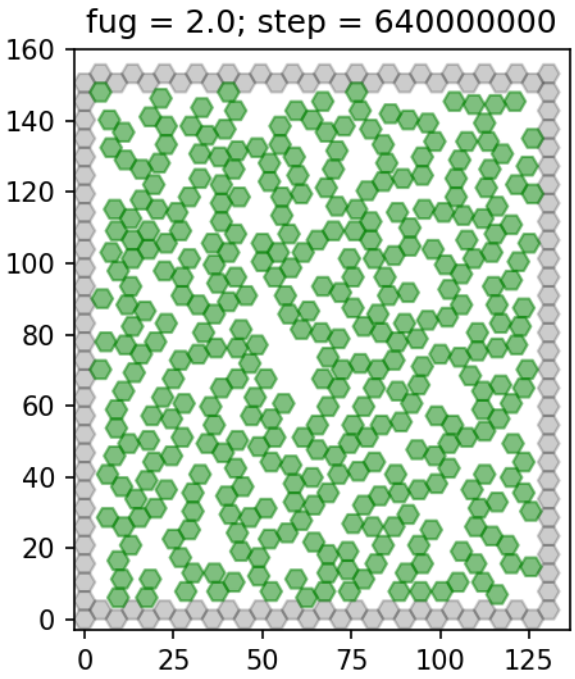

Figure 24: A configuration of the simulation after 6.4e8 steps, for $\mu = 2.0$

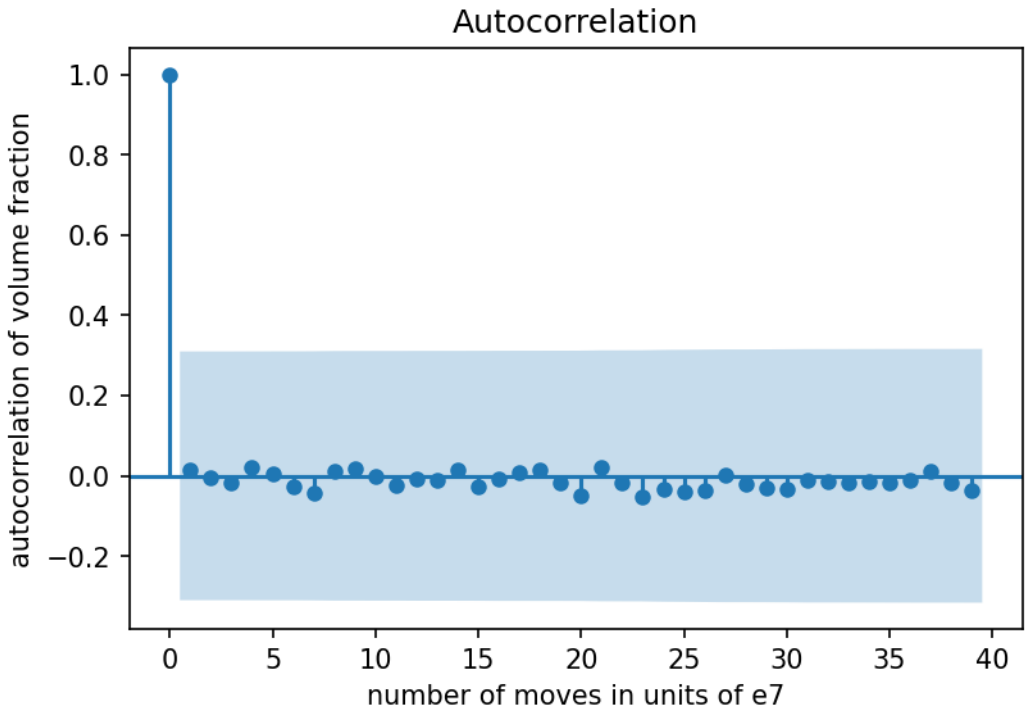

Figure 25: The autocorrelation $R(k)$ vs. number of Monte Carlo steps k, for ψ the volume fraction.

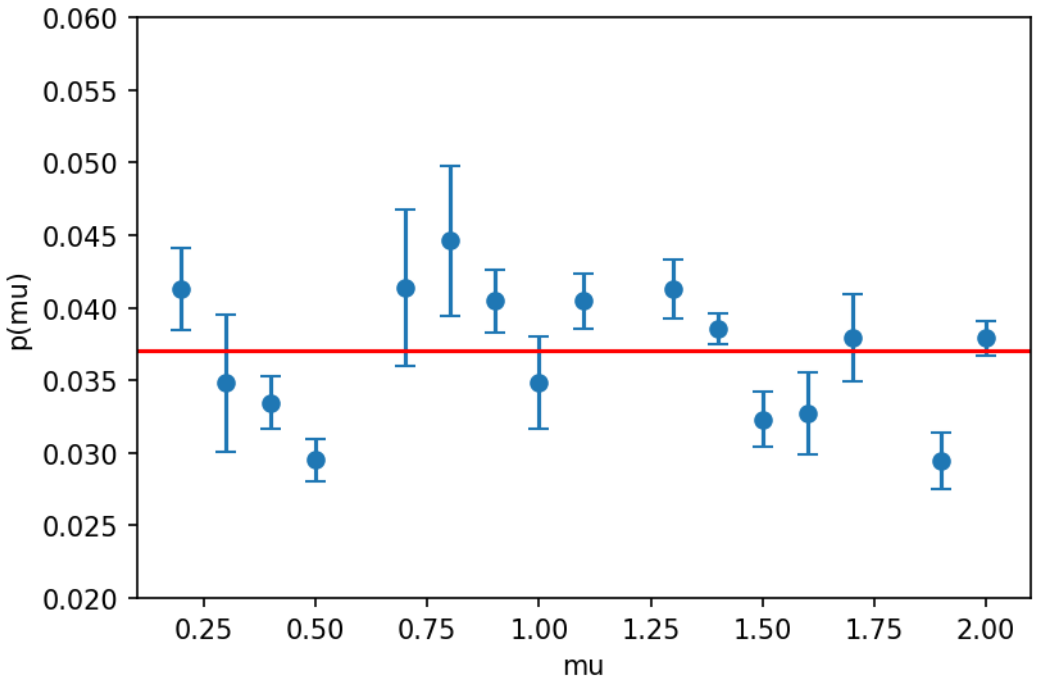

Figure 26: Here we see the calculated $p_M(\mu)$ for different values of μ between 0.1 and 2.0. The red line has a value of $1/27$, which is $1/3s^2$ for $s = 3$; the expected value for $p_M(\mu)$.

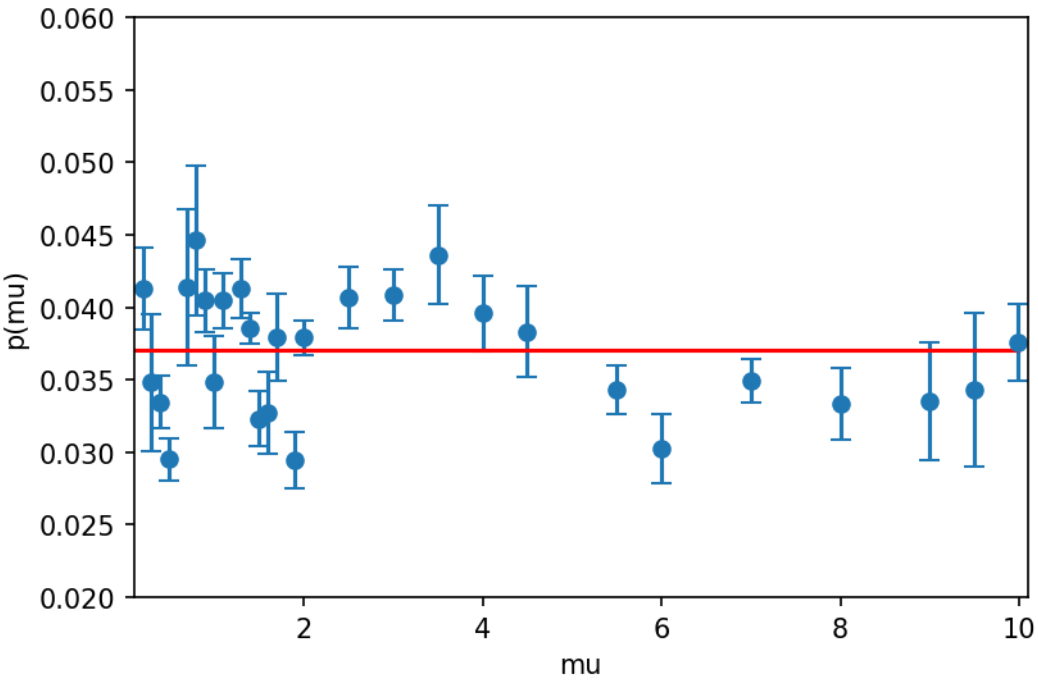

Figure 27: Here we see the calculated $p_M(\mu)$ for different values of μ between 0.1 and 10.0. The red line has a value of $1/27$, which is $1/3s^2$ for $s = 3$; the expected value for $p_M(\mu)$.

Part 2
Non-equilibrium Model

In this section, we discuss a non-equilibrium case of the granular hard hexagon model, and in particular, simulations of the model. We will be in a similar system as in the equilibrium model, but instead of requiring the granular constraints, we introduce two parameters that control gravity and friction. Our main goal is to study metastability in this model.

1 The Granular Hard Hexagon Model Revisited

Similar to the equilibrium part, we consider the granular model which is an adaptation of the hard hexagon model with added effects of gravity and friction. Since we are now interested in a non-equilibrium system, instead of adding a granular constraint as we did in the equilibrium case, we now add the gravity and friction effects in a different manner. We will consider a simulation approach to this model. Our main goal is to study meta-stable states in the model, and under which conditions a meta-stable state transitions into another state.
Again, we consider an infinite triangular lattice Λ with hard-core regular hexagons, where the hexagons are centred on the lattice. We consider a volume V that is bounded on the bottom by hexagons of the boundary structure A, and the rest of the borders are straight boundaries. We add the granularity to the model by adding two granular parameters: gravity, and friction. These influence the possible movements of any hexagons in the system, which make for four distinct possibilities for movement, as seen in Fig. 28. Without granular parameters playing a role, we let any hexagon in the system take a random walk with uniform probability for each of the six directions, and reject a move that leads to overlapping. The gravity and friction parameters change these probabilities depending on the direction and the position of the hexagon.

- The gravity parameter g is the amount of probability that is removed from 'going up' and adds it to 'going down', making the random walk of the hexagons have a downward drift.
- The friction parameter f is the amount of probability that is removed from moving in any direction and added to staying still, provided that the hexagon in question is sitting on at least one other hexagon

Making this explicit, and looking at Fig. 28, these are the probabilities for moving a hexagon into a direction in the following regions:

- Region I: $p = \frac{1}{6} - \frac{1}{2}g - \frac{\delta_{bdd}}{2}f,$
- Region II: $p = \frac{1}{6} - \frac{\delta_{bdd}}{2}f,$
- Region III: $p = \frac{1}{6} + \frac{1}{2}g - \frac{\delta_{bdd}}{2}f,$

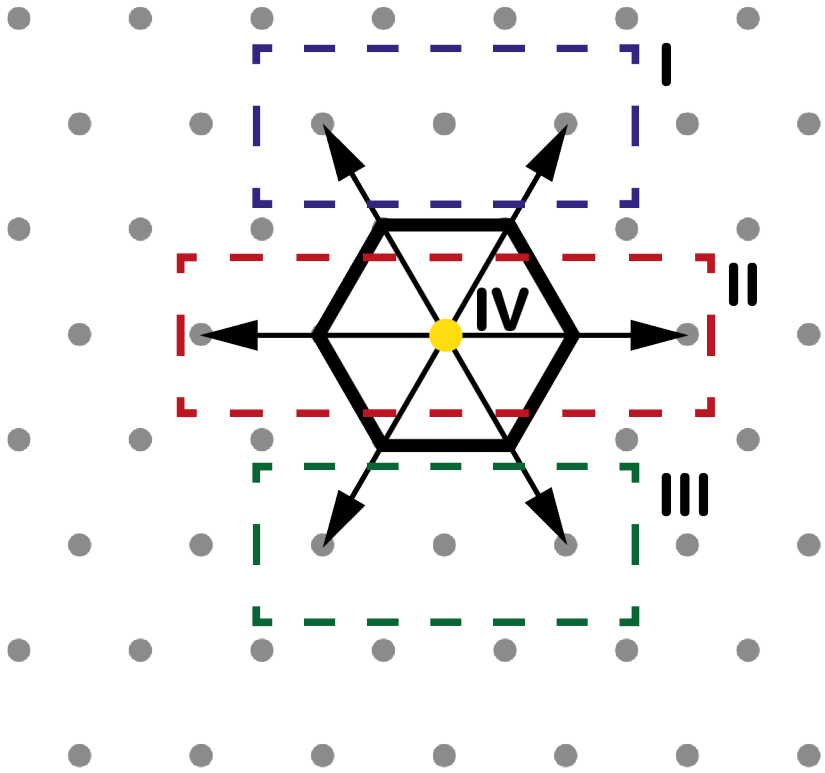

Figure 28: The four regions noted above categorise the possible moves a hexagon can make. Region I-III represent an actual move of the hexagon, whereas region IV signifies the hexagon staying still.

- Region IV: $p = \dfrac{3\delta_{bdd}}{2} f,$

where $\delta_{bdd} = 1$ if the hexagon in question shares a lower edge with an upper edge of at least one other hexagon, and $\delta_{bdd} = 0$ if not. Region IV corresponds to the hexagon not moving. As during the simulation, no particles get added or removed, we start with a certain number of particles and track the density in the lower third of the volume. A starting configuration and ending configuration can be seen in Fig. 29

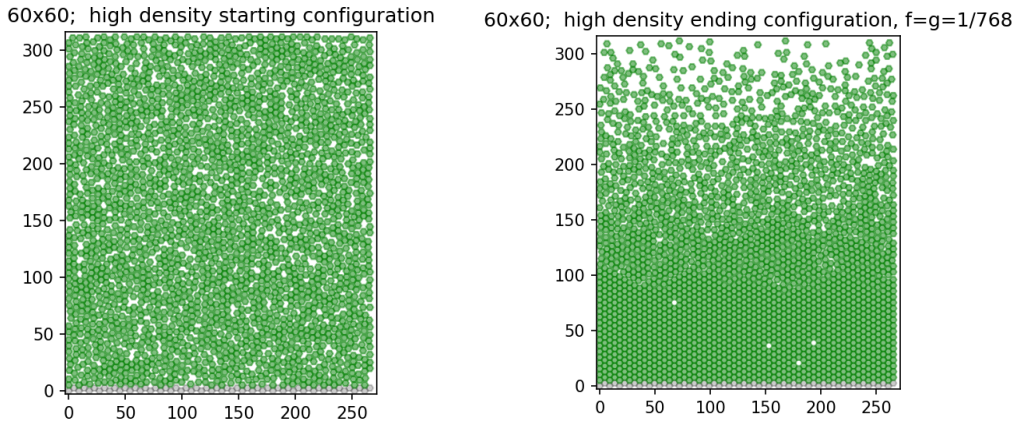

(a) (b)

Figure 29: In (a), we see the starting configuration for a 60x60 high density simulation, with 2500 'free' hexagons, and 60 boundary hexagons. In (b), we see typical configuration after running the simulation, where $f = g = 1/768$.

As we are interested in looking at meta-stability and co-existence of different states in the model, we only made the bottom boundary to be a hexagonal boundary, and the other three edges of the simulated system are straight. As this way the sides will not prefer one hexagon structure over another, this will help find possible co-existences of different states.
There are two important statistics we track throughout the simulation: the first is the particle density of the lower third of the volume, and the second is the ratio of hexagons with the boundary structure in the lower third of the volume (which we will refer to as the 'order parameter'). As we have a downward drift in the random walk thanks to the addition of gravity, we expect the particle density on the lower part of the volume to go up when two co-existing states collapse into a single state. Sudden jerks in this statistic would mean a change in the states in the system. The tracking of the amount of boundary-structure hexagons in the system helps to see any possible influence of the boundary on the rest as the system.

The particulars of our simulations are as follows:

- The volume V is either 30x30 or 60x60 hexagons.
- The starting particle density $\rho \in \{0.29, 0.56, 0.70\}$.
- The gravity parameter $g = 1/384$ for the 30x30 model and either $g = 1/384$ or $g = 1/768$ for the 60x60 model.

- The friction parameter $f \in \{1/24, 1/48, 1/96, 1/192, 1/384\}$ for the 30x30 model, and $g \in \{1/48, 1/192, 1/768\}$ for the 60x60 model.

The f, g parameters are chosen as such to introduce a small gravitational pull and vary the influence of friction, mimicking granular matter while making sure that the hexagons can move enough to allow for phase transitions of a region of hexagons. During preliminary simulations, we found that there were no moments of 'collapse' into another state, as seen in Fig. 30. This seems counterintuitive, as there is a constant downward drift because of the gravity. To explore this behaviour further, the main simulations changed the gravity parameter g every 1e8 steps for 30x30 and every 2.5e8 steps for 60x60 by either adding or removing 1/384 for the 30x30 and 1/768 for the 60x60 to see if it would induce a different state. In total, the 30x30 simulations ran for 5e8 steps, and the 60x60 simulations ran for 1.25e9 steps.
A couple of these simulations illustrating the found behaviour can be seen in Fig. 31 and 32 . The rest will be found in the appendix. An interesting behaviour that we can see in the figures is that the systems are very stable under a constant gravity parameter, and when the gravity parameter changes, the system reacts very quickly and becomes very stable in a different state.

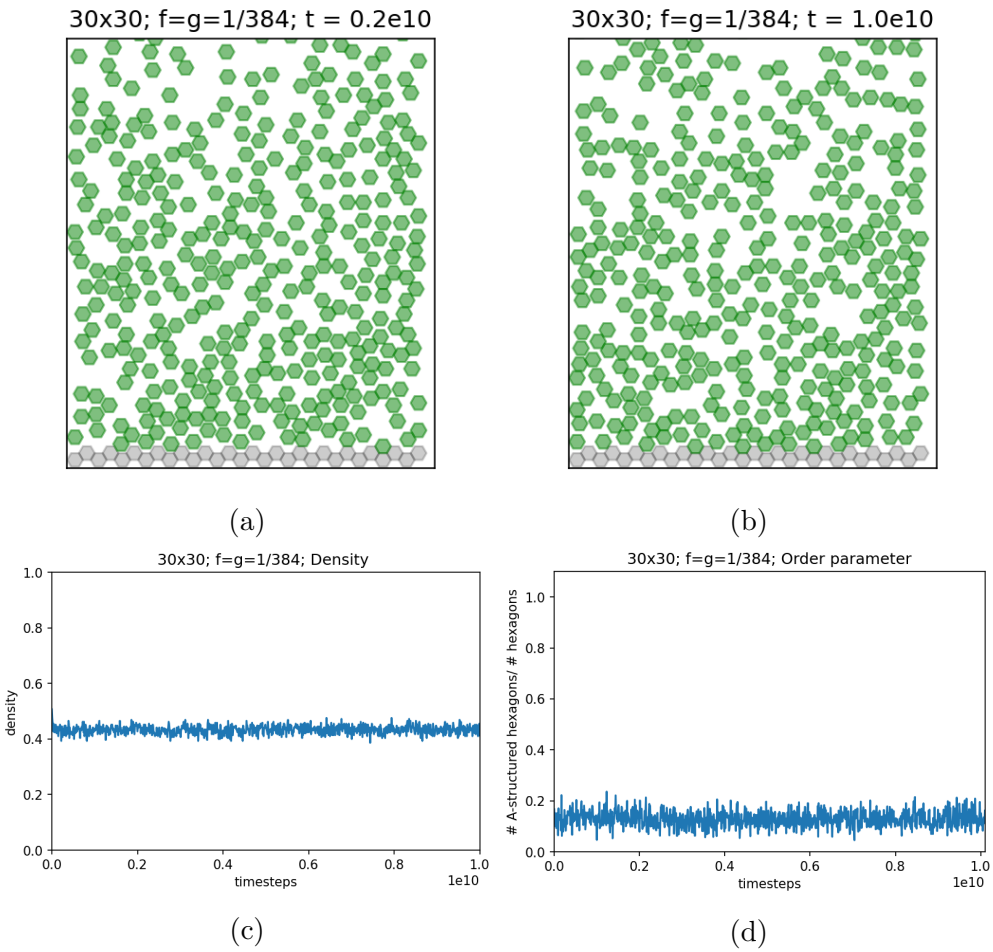

Figure 30: A preliminary simulation of a 30x30 system with 462 'free' hexagons and 30 boundary hexagons. In (a) and (b) we see two snapshots how the system looked at timestep 2e9 and 1e10. It should be noted that there is no distinctive difference between the two configurations. In (c), we see that the density of the lower third of the volume stays in a tight band around 0.42, and similarly the order parameter tracking the amount of hexagons having the boundary structure does not meaningfully change over time.

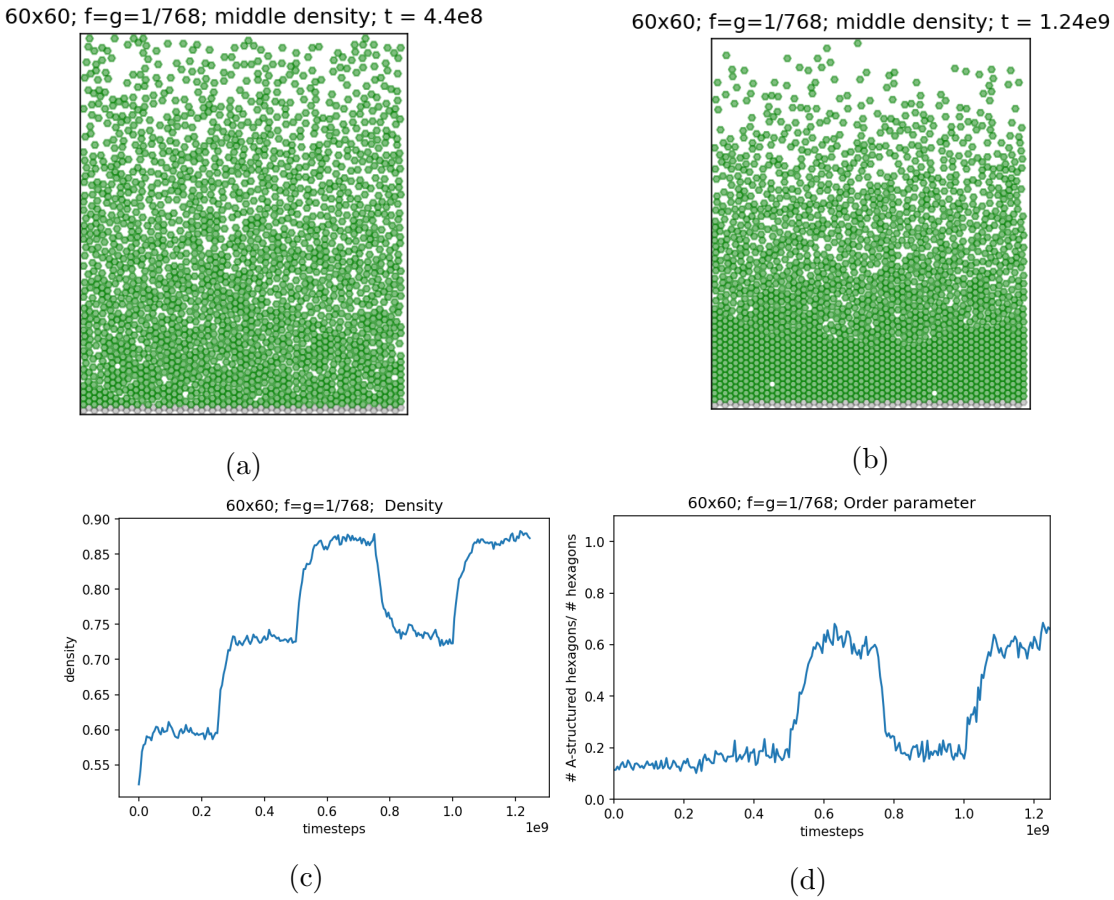

Figure 31: The simulation for a 60x60 system with 2000 'free' hexagons and 60 boundary hexagons. We see in (a) and (b) two snapshots of the simulated system at timestep 4.4e8 and 1.24e9. In (c) we see the plot of the density of the lower third of the volume. Noting that the gravity parameter g changes every 2.5e8 steps, we see very steep changes in the density whenever the parameter g is changed. Something interesting to note is that when g gets lowered, there is almost no relaxation time. We see similar behaviour for the order parameter plot in (d).

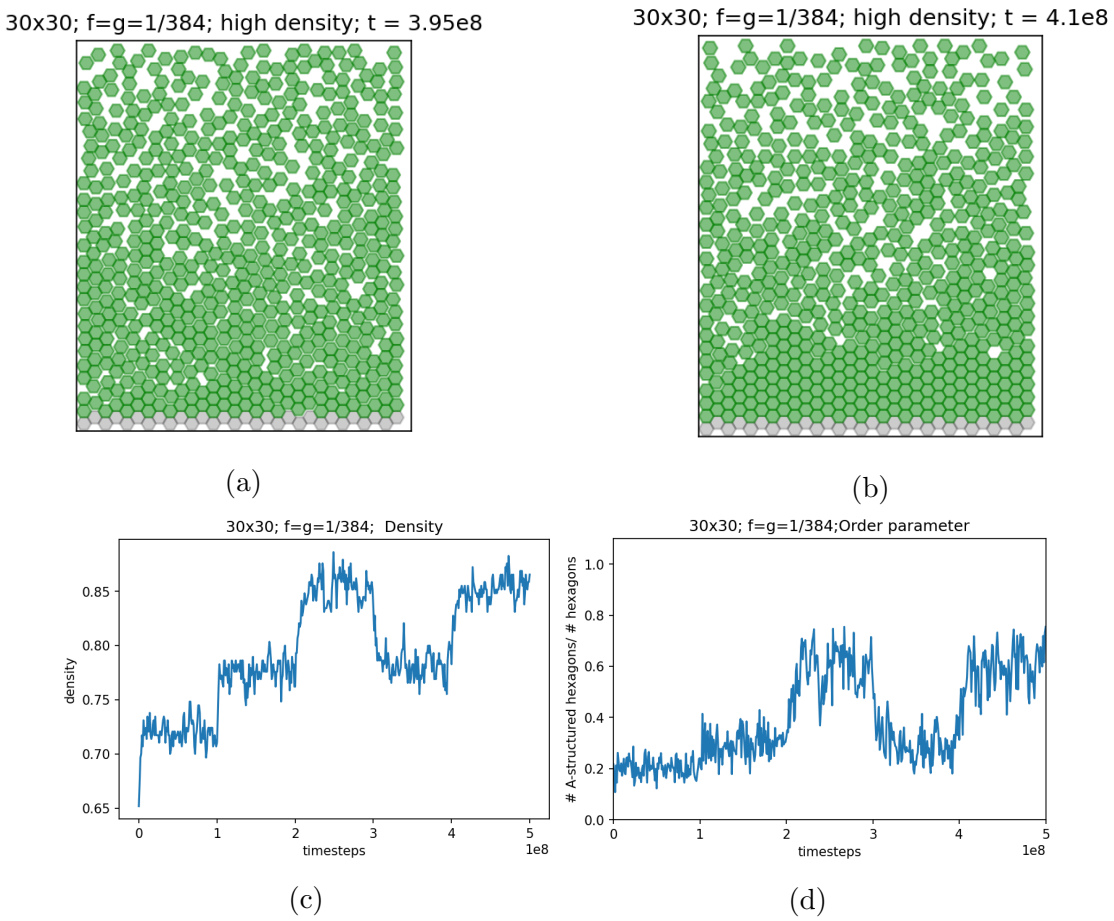

Figure 32: The simulation for a 30x30 system with 624 'free' hexagons and 30 boundary hexagons. We see in (a) and (b) two snapshots of the simulated system at timestep 3.95e8 and 4.1e8. In (c) we see the plot of the density of the lower third of the volume. Noting that the gravity parameter g changes every 1e8 steps, we see very steep changes in the density whenever the parameter g is changed. Something interesting to note is that when g gets lowered, there is almost no relaxation time. We see similar behaviour for the order parameter plot in (d).

Part 3
Discussion and conclusion

1 Discussion and outlook

In this thesis, we discussed the hard hexagon model modified to model granular matter, both in theory and via simulation. We will now discuss our findings and any possible problems, improvements and an outlook for further research.

1.1 Results

1.1.1 Equilibrium model

In the first part of our discussion of the equilibrium granular hexagon model, we have proven that for a large enough μ, hexagons will not be centred equiprobably on each of the lattices, but instead are influenced by the boundary of the system, effectively resulting in an ordered state of the system. We conjectured that for a small enough μ we would have a disordered phase, and simulated the system for a range of small μ. The results from the simulations supported the conjecture, making the hypothesis that there is a order-disorder transition in the system that is facilitated by different values of μ.
The error in the plot of the probability $p(\mu)$ (Fig. 26, **??**) is calculated by looking at the standard deviation of the calculated value for a timestep, so for $p_{M+1d} - p_M$ with M some number of timesteps and d the step size of the measurements. This can be improved by doing multiple simulations and combining the results. This was not done because of time constraints and a problem with using the available cluster server. As stated earlier, we did not find a phase transition in the range of μ we looked at, which is contrary to what we expected, going off of [AR10]. This can either be because the range of our simulation in which we'd see a phase transition is for a higher μ than in the Aristoff simulation; the simulation needed to run longer to see the behaviour, as the Aristoff simulation ran for an order of magnitude longer than we ran our simulation; or there could be a fault in the code preventing this behaviour to occur. As we tried to make our simulation as close to the Aristoff as possible, it seems odd that our range for μ would be so off. The most likely explanation would be the running time, as for a high μ, it could be that it takes longer for the boundary effect to move through the simulation than we typically simulated for.

1.1.2 Non-equilibrium model

Our main goal of the study of the non-equilibrium model was to find out under which circumstances large regions of different states could co-exist. Although we did not find this, the results of the simulations show very interesting behaviour: even with a downward drift in the model, the system seems to not show this (by having the lower third of the system become denser) over time. This can be because of various reasons, the most immediate being that the simulations weren't large enough. Making the gravity parameter larger had a direct influence on the state of the system, showing that there is a state of the system where our

original configuration could end up, provided that we would wait long enough. However, when the gravity parameter is changed back to its original value, the state of the system almost immediately reverts to the original state as well. If this 'higher gravity' state would be the more stable of the two, we'd expect that it would take a bit of time for it to revert back to the original state, and this relaxation time would be measurable. This is not the case, however, signifying that there are more causes. Another possible explanation would be that the system can be characterised as a lot of different 'surfaces' on top of each other. When we consider a system of hexagons with a higher density in the lower third, we can look at the surface of this conglomerate, where hexagons are more free to move than the ones below them, as they are less obstructed by the hexagons above them. For a configuration with a small enough gravity parameter g, we can characterise the more bunched up hexagons by considering each layer as a 'surface' with a certain mobility. Provided that there are enough of these layers, any one of these layers -with the exception of one at the top or bottom- will have a similar amount of mobility. This then results in the system not changing into more dense states over time, even when there is a constant downward drift by virtue of the gravity parameter.

1.2 Improvements

An obvious first improvement of our numerical section is to do more simulations and combining the results. Doing simulations for different sizes of volume and hexagon radius s would also be an interesting check, as one would expect the behaviour to stay the same in the long term. These have not been done because of time constraints and availability of computers to run them.
The current code that was used for the simulations can be improved by tracking the changes in the system, rather than tracking the individual hexagons as is currently the case. This can be done by characterising the volume as a giant matrix and changing the elements depending on where a hexagon is located, instead of tracking the positions of each hexagon. This will speed up the simulations.
A third problem we encountered that can be improved is the way of running the simulations; most of the simulations have been run on a laptop, and even though the later simulations have been ran on the ITP cluster server, a part of them -all on the same 'subcluster'- did not complete running, which can be seen by the gaps in 27 here and there.

1.3 Further research and outlook

As stated above, the simulations can be improved quite easily to make a stronger case for the phase transition in the equilibrium case.
An interesting area to spend more time on would be the analytical argument for the disordered state in the low-density regime of the equilibrium model. This has not been done before as the method of taking an established argument in equilibrium statistical mechanics and applying int to a more complicated granular setting is not doable for the low-density regime, as for low-densities, granular matter cannot exist. Having a compelling analytical argument for a disordered phase at low densities would circumvent the use of simulations entirely, and is certainly an interesting and logical continuation of this thesis.

Finally, a very interesting area to continue this thesis in is the behaviour of the non-equilibrium granular hexagon model. The behaviour we have seen is not necessarily intuitive and also does not have a very clear reason for it. Exploring the reasons for this behaviour in the non-equilibrium model will be worth looking into as a possible continuation of this research.

2 Conclusion

In this thesis, we described the research into granular matter; specifically a equilibrium and a non-equilibrium version of a two-dimensional hard hexagon model with added rules to mimick granular behaviour. We introduced the hard hexagon model and rigorously worked out the details of the Peierls' argument proof of the existence of a phase transition in the non-granular hard hexagon model found in [HP73]. Using this, we proved the existence of a phase transition in the equilibrium granular hard hexagon model, and that the ordered phase of the model is found for large enough μ. To provide an argument for the existence of the disordered phase at a low μ. These findings agree with [AR11].
We also did a numerical study of a non-equilibrium version of the granular hard hexagon model with the goal of finding under which circumstances meta-stability can arise. We did not find an answer to this; instead we found that the states themselves were incredibly parameter-dependent, and we posed possible reasons for this behaviour.

3 Acknowledgements

I would like to thank Cristian Spitoni for his supervision on this project, for the weekly meetings and the interesting discussions. I would also like to thank René van Roij for being the second reader.

References

[LY52] Tsung-Dao Lee and Chen-Ning Yang. "Statistical theory of equations of state and phase transitions. II. Lattice gas and Ising model". In: *Physical Review* 87.3 (1952), p. 410.

[Dob65] Roland L Dobrushin. "Existence of a phase transition in two-dimensional and three-dimensional Ising models". In: *Theory of Probability & Its Applications* 10.2 (1965), pp. 193–213.

[Dob67] Roland L Dobrushin. *Existence of phase transitions in models of a lattice gas.* Tech. rep. Moscow State University Moscow Russia, 1967.

[HP73] Ole J Heilmann and Eigil Praestgaard. "Phase transition of hard hexagons on a triangular lattice". In: *Journal of Statistical Physics* 9.1 (1973), pp. 23–44.

[Hei74] Ole J Heilmann. "The use of Reflection as Symmetry Operation in Connection with Peierls' argument". In: *Communications in Mathematical Physics* 36.2 (1974), pp. 91–114.

[EO89] Sam F Edwards and RBS Oakeshott. "Theory of powders". In: *Physica A: Statistical Mechanics and its Applications* 157.3 (1989), pp. 1080–1090.

[Rad07] Charles Radin. "Random close packing of granular matter". In: *arXiv preprint arXiv:0710.2463* (2007).

[Sch+07] Matthias Schröter et al. "Phase transition in a static granular system". In: *EPL (Europhysics Letters)* 78.4 (2007), p. 44004.

[AR10] David Aristoff and Charles Radin. "Random close packing in a granular model". In: *Journal of Mathematical Physics* 51.11 (2010), p. 113302.

[AR11] David Gregory Aristoff and Charles Radin. "Ordering in Dense Packings". In: (2011).

[Bax16] Rodney J Baxter. *Exactly solved models in statistical mechanics*. Elsevier, 2016.

[Rie+18] Frank Rietz et al. "Nucleation in sheared granular matter". In: *Physical review letters* 120.5 (2018), p. 055701.